Structured Nyquist Correlation Reconstruction for DOA Estimation With Sparse Arrays

Chengwei Zhou, *Member, IEEE*, Yujie Gu, *Senior Member, IEEE*, Zhiguo Shi, *Senior Member, IEEE*, and Martin Haardt, *Fellow, IEEE*

***Abstract*—Sparse arrays are known to achieve an increased number of degrees-of-freedom (DOFs) for direction-of-arrival (DOA) estimation, where an augmented virtual uniform array calculated from the correlations of sub-Nyquist spatial samples is processed to retrieve the angles unambiguously. Nevertheless, the geometry of the derived virtual array is dominated by the specific physical array configurations, as well as the deviation caused by the practical unforeseen circumstances such as detection malfunction and missing data, resulting in a quite sensitive model for virtual array signal processing. In this paper, we propose a novel sparse array DOA estimation algorithm via structured correlation reconstruction, where the Nyquist spatial filling is implemented on the physical array with a compressed transformation related to its equivalent filled array to guarantee the general applicability. While the unknown correlations located in the whole rows and columns of the augmented covariance matrix lead to the fact that strong incoherence property is no longer satisfied for matrix completion, the structural information is introduced as a priori to formulate the structured correlation reconstruction problem for matrix reconstruction. As such, the reconstructed covariance matrix can be effectively processed with full utilization of the achievable DOFs from the virtual array, but with a more flexible constraint on the array configuration. The described estimation problem is theoretically analyzed by deriving the corresponding Cramér-Rao bound (CRB). Moreover, we compare the derived CRB with the performance of the virtual array interpolation-based algorithm. Simulation results demonstrate the effectiveness of the proposed algorithm in terms of DOFs, resolution, and estimation accuracy.**

***Index Terms*—Direction-of-arrival estimation, Nyquist spatial filling, sparse arrays, structured correlation reconstruction.**

Manuscript received 28 June 2022; revised 30 November 2022 and 11 February 2023; accepted 24 February 2023. Date of publication 1 March 2023; date of current version 31 May 2023. The associate editor coordinating the review of this manuscript and approving it for publication was Dr. Monica F. Bugallo. The work of Chengwei Zhou and Zhiguo Shi was supported in part by the National Natural Science Foundation of China under Grants 62271444, 61901413, and U21A20456, in part by the Zhejiang Provincial Natural Science Foundation of China under Grant LZ23F010007, in part by Zhejiang University Education Foundation Qizhen Scholar Foundation, and in part by the 5G Open Laboratory of Hangzhou Future Sci-Tech City. *(Corresponding author: Zhiguo Shi.)*

Chengwei Zhou and Zhiguo Shi are with the College of Information Science and Electronic Engineering, Zhejiang University, Hangzhou, Zhejiang 310027, China, and also with Key Laboratory of Collaborative Sensing and Autonomous Unmanned Systems of Zhejiang Province, Hangzhou, Zhejiang 310015, China (e-mail: zhouchw@zju.edu.cn; shizg@zju.edu.cn).

Yujie Gu is with the Advanced Safety and User Experience, Aptiv, Agoura Hills, CA 91301 USA (e-mail: guyujie@hotmail.com).

Martin Haardt is with the Communications Research Laboratory, Ilmenau University of Technology, D-98684 Ilmenau, Germany (e-mail: martin.haardt@tu-ilmenau.de).

Digital Object Identifier 10.1109/TSP.2023.3251110

I. Introduction

DIRECTION-OF-ARRIVAL (DOA) estimation using sensor arrays plays a fundamental role in a broad range of applications, including radar, acoustics, speech, medical imaging, wireless communications, etc [1], [2], [3], [4], [5], [6]. Generally, the spatial signals are uniformly sampled within the framework of the Nyquist-Shannon sampling theorem for multichannel signal processing, where a uniform linear array (ULA) is the most popular array configuration. While the aperture of the ULA is limited by the number of physical sensors, the idea of sparse sensing has been developed by processing sub-Nyquist spatial samples to overcome the performance bottlenecks. Since sub-Nyquist spatial sampling provides an enhanced resolution with an increased number of degrees-of-freedom (DOFs) beyond the Nyquist sampling-based approaches [7], [8], [9], [10], [11], [12], exploiting sparse arrays for DOA estimation has become a research hotspot, where coprime arrays [13] and nested arrays [14] are the most representative systematically-designed configurations.

Virtual array signal processing techniques are the mainstream solution for DOA estimation with sparse arrays, where the second-order correlation statistics corresponding to an enlarged virtual ULA are processed in the virtual domain [15], [16], [17], [18]. As such, the model variation from Nyquist to sub-Nyquist sampling can be effectively handled for an unambiguous angle retrieval. Nevertheless, it should be noted that the geometry of a virtual array is dominated by the sparse array configurations, which can be categorized as fully augmentable arrays [19] and partially augmentable arrays [20]. As compared to the fully augmentable arrays which have a contiguous virtual array geometry, the partially augmentable arrays do not possess an ideal virtual ULA. A typical solution to cope with a non-uniform virtual array is simply extracting its contiguous segment for the subsequent processing [21]. Although the segmented virtual ULA still has more elements than the number of physical sensors in the sparse array, a performance loss is inevitable due to the removal of correlation statistics corresponding to the discontiguous virtual sensors. On the other hand, since a specific virtual sensor usually corresponds to multiple lags in the derived difference coarray, the correlation calculated from a finite number of sparse array received signals varies [22]. Therefore, how to properly process the available correlations that are calculated from the sub-Nyquist spatial samples to match the Nyquist sampling-based model is a critical task for sparse array DOA estimation.

In order to make full use of the discontiguous virtual array, the idea of spatial interpolation has been introduced to the virtual domain for generating a ULA containing all the derived virtual sensors, where both matrix completion and matrix reconstruction principles have been adopted for the retrieval of the covariance matrix corresponding to the interpolated virtual ULA [23], [24], [25], [26], [27], [28]. With the optimized augmented covariance matrix from virtual array interpolation, all the sub-Nyquist correlations can be effectively processed within the Nyquist sampling rate in the virtual array domain. On the other hand, to maintain a desirable virtual array geometry for processing, the configuration of the sparse array has been optimally designed with specific structural constraints [29], [30], [31]. As such, the properties of both, the physical array and its corresponding virtual array, are optimized to achieve a lower mutual coupling, a lower sensor redundancy, a longer contiguous virtual array, etc. Furthermore, following the dynamic optimization principle, the concept of sparse array motions has been proposed to increase the number of achievable DOFs and contiguous lags for DOA estimation [32], whereas the antenna selection technique dynamically optimizes the sparse array configuration to maintain a given performance guarantee [33]. Moreover, the characteristics of virtual difference coarrays have been optimized by considering the space-frequency domain for multi-dimensional DOA-range parameter joint estimation [34]. Nevertheless, all these efforts in the state-of-art literature are based on a deterministic array configuration. While the geometry of the virtual array is determined by the sparse array configuration, in addition to the restricted physical array configuration in practical usage, unforeseen circumstances such as detection malfunction, sensor failure, and missing data also lead to a quite sensitive geometry in the virtual domain. As such, a random change of the deterministic sparse array configuration will results in a corruption of the contiguous virtual array geometry, leading to an indeterminate signal model. Therefore, it is urgent to develop a generalized framework to effectively process the whole sub-Nyquist correlations for DOA estimation with sparse arrays.

In this paper, we propose a novel sparse array DOA estimation algorithm via structured correlation reconstruction. Instead of deriving the virtual array from the physical array as the conventional methods did, we shift the focus to the physical array domain for generating an equivalent ULA, which is accomplished by filling presumed sensors on the missing Nyquist sampling positions. With an established compressed transformation relationship, the covariance matrix of the assumed ULA is augmented from the sample covariance matrix, where all the correlations calculated from the received signals of the sparse array are taken into account. While the unknown entries are located in entire rows and columns that correspond to the filled sensors, the strong incoherence property is not satisfied for the augmented covariance matrix, indicating that the matrix completion principle becomes infeasible [35]. To address this technical bottleneck, the Hermitian Toeplitz structure of the ULA-based covariance matrix is incorporated as a priori information to formulate a structured correlation reconstruction problem for the retrieval of the unknown entries in the augmented covariance matrix. With the optimized covariance matrix corresponding to the assumed ULA, the Nyquist sampling-based processing can be applied to resolve off-grid sources with an increased number of DOFs. An equivalent performance relationship between the proposed Nyquist spatial filling-based approach and the virtual array interpolation-based approaches is analyzed, and the performance bound for the estimation of DOAs is also theoretically derived. Simulation results are presented to validate the effectiveness of the proposed DOA estimation algorithm.

TABLE I
LIST OF NOTATIONS

Symbol	Description
$a, \boldsymbol{a}, \boldsymbol{A}$	Scalar, vector, and matrix
$(\cdot)^*, (\cdot)^{\mathrm{T}}, (\cdot)^{\mathrm{H}}$	Conjugation, transpose, and conjugate transpose
$E[\cdot]$	Statistical expectation
$\mathrm{diag}(\cdot)$	Diagonal transformation between a column vector and its corresponding diagonal matrix
$\mathrm{vec}(\cdot)$	Vectorization
$\otimes, \odot$	Kronecker product, Khatri-Rao product
$\succeq$	Matrix inequality
$\lVert\cdot\rVert_F, \lVert\cdot\rVert_*$	Frobenius norm, nuclear norm
$\jmath = \sqrt{-1}$	Imaginary unit
$\mathcal{P}_\Omega(\cdot)$	Projection operation with the corresponding positions indexed by set Ω
$\mathrm{Toep}(\boldsymbol{a})$	Hermitian Toeplitz matrix with $\boldsymbol{a}$ as its first column
$\mathrm{Tr}(\cdot), \mathrm{rank}(\cdot)$	Trace, rank
$\boldsymbol{A}^{-1}, \lambda_i(\boldsymbol{A})$	Inverse, the i-th eigenvalue of $\boldsymbol{A}$
$\lvert\mathbb{A}\rvert$	Cardinality of $\mathbb{A}$
$\mathbb{A}_+$	Non-negative subset of $\mathbb{A}$
$\mathbb{C}, \mathbb{R}$	Set of complex number, set of real number
$\boldsymbol{I}$	Identity matrix
$\mathbf{0}$	Zero vector or matrix

To be specific, the main contributions of this work are summarized as follows.

- We present a Nyquist spatial filling approach to the physical array for DOA estimation with generalized sparse arrays, where the established compressed transformation guarantees the full utilization of sub-Nyquist correlations without limiting the deterministic array configuration.
- We formulate a correlation reconstruction problem with matrix structure constraints to retrieve the whole rows and columns of the augmented covariance matrix corresponding to the presumed sensors, such that the Nyquist sampling-based methods can be effectively processed.
- We derive the Cramér-Rao bound (CRB) for DOA estimation from the reconstructed covariance matrix of a presumed ULA, based on which the equivalence relationship to the virtual array interpolation-based algorithms is verified.

The rest of this paper is structured as follows. In Section II, the preliminaries of the sparse array signal model are presented. In Section III, the proposed structured correlation reconstruction-based DOA estimation algorithm is described, and its theoretical performance analysis is presented in Section IV. In Section V, numerical simulations are conducted for performance comparison, and the conclusions are drawn in Section VI. The notations throughout this paper are listed in Table I.

II. Sparse Array Signal Model

By focusing on sensor arrays, sub-Nyquist spatial sampling as well as its diverse variants in practical applications including sensor failure can be abstracted as a sparse array configuration as shown in Fig. 1(a). In particular, the Nyquist sampling positions $\mathbb{U}$ represented by the dashed squares have an inter-element spacing of unit d, which is equals to half a wavelength, i.e., the

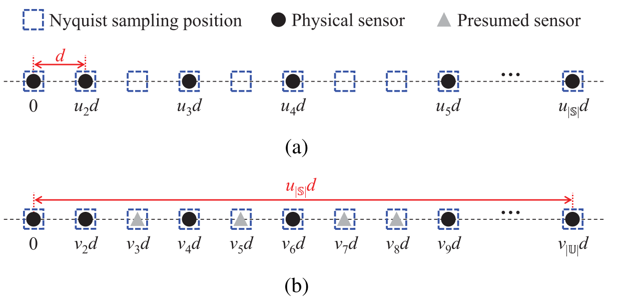

Fig. 1. Illustration of Nyquist spatial filling for sparse arrays. (a) $\mathbb{S}$: Sparse array; (b) $\mathbb{U}$: Presumed ULA.

maximum distance satisfying the Nyquist spatial sampling rate. The sensors' positions of a sparse array $\mathbb{S}$ constitute a subset of $\mathbb{U}$, i.e., $\mathbb{S} = \{u_1 d, u_2 d, \ldots, u_{|\mathbb{S}|} d\} \subset \mathbb{U}$ with the first element as the reference (e.g., $u_1 = 0$). Due to the sparse deployment, the spacings between adjacent sensors in $\mathbb{S}$ are usually larger than d.

Assuming that there are K far-field narrowband and uncorrelated sources illuminating the sparse array $\mathbb{S}$ from distinct directions $\boldsymbol{\theta} = [\theta_1, \theta_2, \ldots, \theta_K]^{\mathrm{T}}$, the received signals in the l-th time slot can be modeled as

$$\boldsymbol{x}(l) = \sum_{k=1}^{K} \boldsymbol{a}_{\mathbb{S}}(\theta_k) s_k(l) + \boldsymbol{n}_{\mathbb{S}}(l) = \boldsymbol{A}_{\mathbb{S}}(\boldsymbol{\theta}) \boldsymbol{s}(l) + \boldsymbol{n}_{\mathbb{S}}(l), \quad (1)$$

where

$$\boldsymbol{a}_{\mathbb{S}}(\theta_k) = \left[1, e^{-\jmath\pi u_2 \sin(\theta_k)}, \ldots, e^{-\jmath\pi u_{|\mathbb{S}|} \sin(\theta_k)}\right]^{\mathrm{T}} \in \mathbb{C}^{|\mathbb{S}|} \quad (2)$$

denotes the steering vector towards θ_k, $\boldsymbol{A}_{\mathbb{S}}(\boldsymbol{\theta}) = [\boldsymbol{a}_{\mathbb{S}}(\theta_1), \boldsymbol{a}_{\mathbb{S}}(\theta_2), \ldots, \boldsymbol{a}_{\mathbb{S}}(\theta_K)] \in \mathbb{C}^{|\mathbb{S}| \times K}$ is the steering matrix of the sparse array $\mathbb{S}$, $\boldsymbol{s}(l) = [s_1(l), s_2(l), \ldots, s_K(l)]^{\mathrm{T}} \in \mathbb{C}^K$ contains the signal waveforms of the K sources, and $\boldsymbol{n}_{\mathbb{S}}(l) \sim \mathcal{CN}(\mathbf{0}, \sigma_n^2 \boldsymbol{I})$ is an independent and identically distributed (i.i.d.) additive Gaussian white noise vector with σ_n^2 representing the noise power.

Accordingly, the array covariance matrix can be expressed as

$$\begin{aligned} \boldsymbol{R}_{\boldsymbol{xx}} &= E\left[\boldsymbol{x}(l)\boldsymbol{x}^{\mathrm{H}}(l)\right] = \sum_{k=1}^{K} \sigma_k^2 \boldsymbol{a}_{\mathbb{S}}(\theta_k) \boldsymbol{a}_{\mathbb{S}}^{\mathrm{H}}(\theta_k) + \sigma_n^2 \boldsymbol{I} \\ &= \boldsymbol{A}_{\mathbb{S}}(\boldsymbol{\theta}) \boldsymbol{P} \boldsymbol{A}_{\mathbb{S}}^{\mathrm{H}}(\boldsymbol{\theta}) + \sigma_n^2 \boldsymbol{I}, \end{aligned} \quad (3)$$

where $\sigma_k^2 = E[|s_k(l)|^2]$ denotes the power of the k-th source, and $\boldsymbol{P} = \mathrm{diag}(\boldsymbol{p}) = \mathrm{diag}([\sigma_1^2, \sigma_2^2, \ldots, \sigma_K^2]^{\mathrm{T}})$ is a diagonal matrix containing the power of K sources. In practical applications, the array covariance matrix $\boldsymbol{R}_{\boldsymbol{xx}}$ is usually estimated by the sample covariance matrix

$$\hat{\boldsymbol{R}}_{\boldsymbol{xx}} = \frac{1}{L} \sum_{l=1}^{L} \boldsymbol{x}(l) \boldsymbol{x}^{\mathrm{H}}(l), \quad (4)$$

where L denotes the number of snapshots.

Compared with ULAs, sparse arrays are capable of breaking through the DOFs limited by the number of physical sensors while offering a higher resolution. Nevertheless, the incomplete signal model resulting from the sub-Nyquist spatial sampling prevents a direct adoption of the conventional Nyquist sampling-based methods to process the formulated signal model $\boldsymbol{x}(l)$. Therefore, it is necessary to explore a general solution to process the signals received by the sparse arrays, such that the advantages brought by the sparse deployment can be effectively maintained.

III. Direction-of-Arrival Estimation for Generalized Sparse Linear Arrays

In this section, we propose a structured correlation reconstruction-based DOA estimation algorithm for generalized sparse linear arrays. First, we focus on the sparse array itself rather than generate a virtual array, and implement the Nyquist spatial filling to generate a presumed ULA, where the transformation relationship between their correlation statistics can be uniquely established. Then, we can retrieve the unknown correlations corresponding to the presumed sensors in the augmented covariance matrix of the presumed ULA by solving a structured correlation reconstruction problem, where the structural information is incorporated as a priori to address the challenges caused by the whole rows and columns of missing elements. As such, the reconstructed covariance matrix corresponding to the presumed ULA can be effectively utilized to perform DOA estimation within the framework of Nyquist spatial sampling.

A. Nyquist Spatial Filling and Compressed Transformation

In order to meet the Nyquist spatial sampling while maintaining the enlarged array aperture offered by the sparse arrays, we propose a Nyquist spatial filling scheme for the generation of a presumed ULA. In particular, as shown in Fig. 1, by filling the presumed sensors represented by the gray triangles into Nyquist sampling positions ranging from 0 to $u_{|\mathbb{S}|} d$ where the physical sensor does not exist, the resulting presumed ULA $\mathbb{U} = \{v_1 d, v_2 d, \ldots, v_{|\mathbb{U}|} d\}$ shown in Fig. 1(b) has the same array aperture of $u_{|\mathbb{S}|} d$ as that of the original sparse array $\mathbb{S}$, where $v_{|\mathbb{U}|} = u_{|\mathbb{S}|}$ and $v_1 = 0$. As such, the discontiguous sparse array $\mathbb{S}$ is transformed into a contiguous uniform array $\mathbb{U}$ with all the elements in $\mathbb{S}$ included.

Since no actual signal is sampled from the positions of $\mathbb{U} - \mathbb{S}$, there is no knowledge about the signal statistics available from these presumed sensors. In order to perform Nyquist sampling-based DOA estimation, it is necessary to activate these presumed sensors by recovering their corresponding signal statistics. Theoretically, the received signals of the presumed ULA $\mathbb{U}$ can be expressed as

$$\boldsymbol{y}(l) = \sum_{k=1}^{K} \boldsymbol{a}_{\mathbb{U}}(\theta_k) s_k(l) + \boldsymbol{n}_{\mathbb{U}}(l) = \boldsymbol{A}_{\mathbb{U}}(\boldsymbol{\theta}) \boldsymbol{s}(l) + \boldsymbol{n}_{\mathbb{U}}(l), \quad (5)$$

where $\boldsymbol{A}_{\mathbb{U}}(\boldsymbol{\theta}) = [\boldsymbol{a}_{\mathbb{U}}(\theta_1), \boldsymbol{a}_{\mathbb{U}}(\theta_2), \ldots, \boldsymbol{a}_{\mathbb{U}}(\theta_K)] \in \mathbb{C}^{|\mathbb{U}| \times K}$ is the steering matrix of the presumed ULA $\mathbb{U}$ with the k-th column

$$\boldsymbol{a}_{\mathbb{U}}(\theta_k) = \left[1, e^{-\jmath\pi v_2 \sin(\theta_k)}, \ldots, e^{-\jmath\pi v_{|\mathbb{U}|} \sin(\theta_k)}\right]^{\mathrm{T}} \quad (6)$$

representing the steering vector towards θ_k, and $\boldsymbol{n}_{\mathbb{U}}(l) \in \mathbb{C}^{|\mathbb{U}|}$ is the additive Gaussian white noise vector with the same statistical character as $\boldsymbol{n}_{\mathbb{S}}(l)$ in (1).

Accordingly, the sparse array received signal $\boldsymbol{x}(l)$ in (1) can be regarded as a compressed sampling of the presumed ULA received signal $\boldsymbol{y}(l)$ in (5), i.e.,

$$\begin{aligned}\boldsymbol{x}(l) = \boldsymbol{\Phi}\boldsymbol{y}(l) &= \sum_{k=1}^{K} \boldsymbol{\Phi}\boldsymbol{a}_{\mathbb{U}}(\theta_k)s_k(l) + \boldsymbol{\Phi}\boldsymbol{n}_{\mathbb{U}}(l) \\ &= \boldsymbol{\Phi}\boldsymbol{A}_{\mathbb{U}}(\boldsymbol{\theta})\boldsymbol{s}(l) + \boldsymbol{\Phi}\boldsymbol{n}_{\mathbb{U}}(l), \end{aligned} \tag{7}$$

where $\boldsymbol{\Phi} \in \mathbb{R}^{|\mathbb{S}|\times|\mathbb{U}|}$ is a sketching matrix containing binary entries 0 and 1. More specifically, the entry of the i-th row and the j-th column of the sketching matrix, $\boldsymbol{\Phi}_{i,j}$, is 1 if and only if the i-th element in $\mathbb{S}$ overlaps with the j-th element in $\mathbb{U}$ (i.e., its $(i, u_i + 1)$-th element is 1), while all the remaining elements are 0, $i = 1, 2, \ldots, |\mathbb{S}|$. As an illustrative example, the sketching matrix relating a sparse array

$$\mathbb{S}_{\text{example}} = \{0, d, 2d, 5d, 7d\} \tag{8}$$

and the corresponding presumed ULA

$$\mathbb{U}_{\text{example}} = \{0, d, 2d, 3d, 4d, 5d, 6d, 7d\} \tag{9}$$

is given by

$$\boldsymbol{\Phi}_{\text{example}} = \begin{bmatrix} 1 & 0 & 0 & 0 & 0 & 0 & 0 & 0 \\ 0 & 1 & 0 & 0 & 0 & 0 & 0 & 0 \\ 0 & 0 & 1 & 0 & 0 & 0 & 0 & 0 \\ 0 & 0 & 0 & 0 & 0 & 1 & 0 & 0 \\ 0 & 0 & 0 & 0 & 0 & 0 & 0 & 1 \end{bmatrix}. \tag{10}$$

In contrast to the conventional compressive sensing method using *random* sensing kernels for dimension reduction, the sketching matrix $\boldsymbol{\Phi}$ is *fixed* for a given sparse array, which lays the foundation for processing the generalized sparse array.

In particular, with the sketching matrix $\boldsymbol{\Phi}$, the sparse array covariance matrix $\boldsymbol{R}_{\boldsymbol{xx}} \in \mathbb{C}^{|\mathbb{S}|\times|\mathbb{S}|}$ in (3) can be reformulated as

$$\boldsymbol{R}_{\boldsymbol{xx}} = \boldsymbol{\Phi} E\left[\boldsymbol{y}(l)\boldsymbol{y}^{\mathrm{H}}(l)\right]\boldsymbol{\Phi}^{\mathrm{H}} = \boldsymbol{\Phi}\boldsymbol{R}_{\boldsymbol{yy}}\boldsymbol{\Phi}^{\mathrm{H}}, \tag{11}$$

where

$$\begin{aligned}\boldsymbol{R}_{\boldsymbol{yy}} = E\left[\boldsymbol{y}(l)\boldsymbol{y}^{\mathrm{H}}(l)\right] &= \sum_{k=1}^{K} \sigma_k^2 \boldsymbol{a}_{\mathbb{U}}(\theta_k)\boldsymbol{a}_{\mathbb{U}}^{\mathrm{H}}(\theta_k) + \sigma_n^2 \boldsymbol{I} \\ &= \boldsymbol{A}_{\mathbb{U}}(\boldsymbol{\theta})\boldsymbol{P}\boldsymbol{A}_{\mathbb{U}}^{\mathrm{H}}(\boldsymbol{\theta}) + \sigma_n^2\boldsymbol{I} \end{aligned} \tag{12}$$

is the theoretical covariance matrix of the presumed ULA $\mathbb{U}$. Since $\boldsymbol{\Phi}$ is a real-valued matrix following $\boldsymbol{\Phi}\boldsymbol{\Phi}^{\mathrm{H}} = \boldsymbol{I} \in \mathbb{R}^{|\mathbb{S}|\times|\mathbb{S}|}$, it will not affect the noise covariance matrix in $\boldsymbol{R}_{\boldsymbol{yy}}$ during dimension reduction. Hence, (11) can be rewritten as

$$\boldsymbol{R}_{\boldsymbol{xx}} = \boldsymbol{\Phi}\boldsymbol{A}_{\mathbb{U}}(\boldsymbol{\theta})\boldsymbol{P}\boldsymbol{A}_{\mathbb{U}}^{\mathrm{H}}(\boldsymbol{\theta})\boldsymbol{\Phi}^{\mathrm{H}} + \sigma_n^2\boldsymbol{I} \tag{13}$$

with $\boldsymbol{\Phi}\boldsymbol{A}_{\mathbb{U}}(\boldsymbol{\theta}) = \boldsymbol{A}_{\mathbb{S}}(\boldsymbol{\theta})$. On the other hand, the sketching matrix $\boldsymbol{\Phi}$ has the property of $\boldsymbol{\Phi}^{\mathrm{H}}\boldsymbol{\Phi} = \boldsymbol{\Lambda}$, where $\boldsymbol{\Lambda} \in \mathbb{R}^{|\mathbb{U}|\times|\mathbb{U}|}$ is a diagonal matrix, and the binary elements on its main diagonal represent the existence of physical sensors in each position of $\mathbb{U}$. As such, the sparse array sample covariance matrix $\hat{\boldsymbol{R}}_{\boldsymbol{xx}} \in \mathbb{C}^{|\mathbb{S}|\times|\mathbb{S}|}$ can be augmented to a presumed uniform array sample covariance matrix $\hat{\boldsymbol{R}}_{\boldsymbol{yy}} \in \mathbb{C}^{|\mathbb{U}|\times|\mathbb{U}|}$ as

$$\tilde{\boldsymbol{R}}_{\boldsymbol{yy}} = \boldsymbol{\Lambda}\hat{\boldsymbol{R}}_{\boldsymbol{yy}}\boldsymbol{\Lambda} = \boldsymbol{\Phi}^{\mathrm{H}}\hat{\boldsymbol{R}}_{\boldsymbol{xx}}\boldsymbol{\Phi}. \tag{14}$$

Obviously, the entries in $\tilde{\boldsymbol{R}}_{\boldsymbol{yy}}$ related to the presumed sensor positions are all zeros, whereas the other entries remain the same as those corresponding correlations in $\hat{\boldsymbol{R}}_{\boldsymbol{xx}}$. As such, the problem of filling the presumed sensors in the spatial domain has been transformed into the problem of retrieving the zero-forced correlations in the augmented covariance matrix $\tilde{\boldsymbol{R}}_{\boldsymbol{yy}} = \boldsymbol{\Lambda}\hat{\boldsymbol{R}}_{\boldsymbol{yy}}\boldsymbol{\Lambda}$. Therefore, it is critical to estimate the correlation of the presumed ULA from the sample covariance matrix $\hat{\boldsymbol{R}}_{\boldsymbol{xx}}$.

B. Structured Nyquist Correlation Reconstruction

According to the structure of the sketching matrix $\boldsymbol{\Phi}$, it is observed that for any $\ell d \in \mathbb{U} - \mathbb{S}$, both $(\ell + 1)$-th row and the $(\ell + 1)$-th column of the augmented covariance matrix $\tilde{\boldsymbol{R}}_{\boldsymbol{yy}}$ in (14) are all-zero vectors. Unfortunately, all-zero vectors either in rows or in columns cannot be effectively retrieved through matrix completion, which essentially exploits the data correlation [35]. In particular, when there is no information available in the entire row or column, the strong incoherence property is not satisfied; hence, there is no optimal solution for such a matrix completion problem.

Note that, due to a finite number of temporal samples, it is not mandatory to keep the calculated correlations same in the retrieved covariance matrix. Therefore, we turn to adopt the principle of matrix reconstruction, where the available correlations are taken as the reference for reconstruction. With the observation that the theoretical covariance matrix of the ULA (e.g., $\boldsymbol{R}_{\boldsymbol{yy}}$ in (12)) is Toeplitz and Hermitian, we propose a structured correlation reconstruction problem

$$\begin{aligned} \min_{\bar{\boldsymbol{R}}_{\boldsymbol{yy}} \in \mathbb{C}^{|\mathbb{U}|\times|\mathbb{U}|}} \quad & \left\| \boldsymbol{\Phi}\bar{\boldsymbol{R}}_{\boldsymbol{yy}}\boldsymbol{\Phi}^{\mathrm{H}} - \hat{\boldsymbol{R}}_{\boldsymbol{xx}} \right\|_F \\ \text{subject to} \quad & \operatorname{rank}\left(\bar{\boldsymbol{R}}_{\boldsymbol{yy}}\right) = K, \\ & \bar{\boldsymbol{R}}_{\boldsymbol{yy}}^{\mathrm{H}} = \bar{\boldsymbol{R}}_{\boldsymbol{yy}}, \quad \bar{\boldsymbol{R}}_{\boldsymbol{yy}} \in \mathbb{T}_{\text{PSD}}^{|\mathbb{U}|} \end{aligned} \tag{15}$$

to reconstruct the covariance matrix corresponding to the presumed ULA $\mathbb{U}$. Here, the objective function aims to minimize the fitting error between the observed sub-Nyquist correlations in the sample covariance matrix $\hat{\boldsymbol{R}}_{\boldsymbol{xx}}$ and those at the corresponding positions of the optimization variable $\bar{\boldsymbol{R}}_{\boldsymbol{yy}}$. The first equality constraint maintains $\bar{\boldsymbol{R}}_{\boldsymbol{yy}}$ a low-rank matrix with its rank equals to the number of sources K, whereas the second equality constraint enforces $\bar{\boldsymbol{R}}_{\boldsymbol{yy}}$ to be a Hermitian matrix. The last constraint indicates that $\bar{\boldsymbol{R}}_{\boldsymbol{yy}}$ is a $|\mathbb{U}|$-dimensional positive semi-definite (PSD) Toeplitz square matrix, owing to non-negative power for both sources and noise. With the constraints of these structural information as a priori, it is possible to retrieve the zero-forced rows and columns in $\tilde{\boldsymbol{R}}_{\boldsymbol{yy}}$.

Alternatively, the proposed optimization problem (15) can be reformulated as

$$\begin{aligned} \min_{\bar{\boldsymbol{R}}_{\boldsymbol{yy}} \in \mathbb{C}^{|\mathbb{U}|\times|\mathbb{U}|}} \quad & \left\| \boldsymbol{\Phi}\bar{\boldsymbol{R}}_{\boldsymbol{yy}}\boldsymbol{\Phi}^{\mathrm{H}} - \hat{\boldsymbol{R}}_{\boldsymbol{xx}} \right\|_F + \mu \operatorname{rank}\left(\bar{\boldsymbol{R}}_{\boldsymbol{yy}}\right) \\ \text{subject to} \quad & \bar{\boldsymbol{R}}_{\boldsymbol{yy}}^{\mathrm{H}} = \bar{\boldsymbol{R}}_{\boldsymbol{yy}}, \quad \bar{\boldsymbol{R}}_{\boldsymbol{yy}} \in \mathbb{T}_{\text{PSD}}^{|\mathbb{U}|}, \end{aligned} \tag{16}$$

where μ is a regularization parameter to balance the covariance fitting error and the rank penalty. However, since the matrix rank is nonconvex, the optimization problem (16) is NP-hard. To address this issue, the nuclear norm is introduced as a convex relaxation of the nonconvex matrix rank. As such, the nonconvex structured correlation reconstruction problem can be relaxed as

Algorithm 1: Proposed Structured Nyquist Correlation Reconstruction-based Sparse Array DOA Estimation.

1: **Input:** Array configuration $\mathbb{S}$, received signals $\{\boldsymbol{x}(l)\}_{l=1}^{L}$.
2: **Output:** Estimated DOAs $\hat{\boldsymbol{\theta}} = [\hat{\theta}_1, \hat{\theta}_2, \ldots, \hat{\theta}_K]^{\mathrm{T}}$.
3: Calculate the sample covariance matrix $\hat{\boldsymbol{R}}_{\boldsymbol{xx}}$ by (4);
4: Perform Nyquist spatial filling on the physical array $\mathbb{S}$ to generate a presumed ULA $\mathbb{U}$;
5: Determine the sketching matrix $\boldsymbol{\Phi}$ based on $\mathbb{S}$ and $\mathbb{U}$;
6: Relate the sample covariance matrix $\hat{\boldsymbol{R}}_{\boldsymbol{xx}}$ to its augmented version $\tilde{\boldsymbol{R}}_{\boldsymbol{yy}}$ via the compressed transformation (14);
7: Solve the convex optimization problem (17) to obtain the optimized covariance matrix $\boldsymbol{R}_{\boldsymbol{yy}}^{\star}$ corresponding to $\mathbb{U}$;
8: Implement Nyquist sampling-based DOA estimation on $\boldsymbol{R}_{\boldsymbol{yy}}^{\star} \in \mathbb{C}^{|\mathbb{U}|\times|\mathbb{U}|}$, e.g., via MUSIC as in (18).

a convex optimization problem

$$\min_{\bar{\boldsymbol{R}}_{\boldsymbol{yy}} \in \mathbb{C}^{|\mathbb{U}|\times|\mathbb{U}|}} \quad \left\| \boldsymbol{\Phi} \bar{\boldsymbol{R}}_{\boldsymbol{yy}} \boldsymbol{\Phi}^{\mathrm{H}} - \hat{\boldsymbol{R}}_{\boldsymbol{xx}} \right\|_F + \mu \left\| \bar{\boldsymbol{R}}_{\boldsymbol{yy}} \right\|_*$$
$$\text{subject to} \quad \bar{\boldsymbol{R}}_{\boldsymbol{yy}}^{\mathrm{H}} = \bar{\boldsymbol{R}}_{\boldsymbol{yy}}, \quad \bar{\boldsymbol{R}}_{\boldsymbol{yy}} \in \mathbb{T}_{\mathrm{PSD}}^{|\mathbb{U}|}, \tag{17}$$

which can be efficiently solved by interior-point methods. Meanwhile, considering the fact that the optimization problem (17) is dedicated to a generalized framework for sparse array configurations, the nonsmooth nuclear norm term $\|\bar{\boldsymbol{R}}_{\boldsymbol{yy}}\|_*$ may cause a nonconvergent iteration process under certain circumstances. As such, the alternating direction method of multipliers solution can also be implemented as a candidate to expedite the solving process.

The optimized solution of (17) $\boldsymbol{R}_{\boldsymbol{yy}}^{\star}$ behaves like the covariance matrix of the presumed ULA $\mathbb{U}$, i.e., $\boldsymbol{R}_{\boldsymbol{yy}}$ in (12), whose steering matrix $\boldsymbol{A}_{\mathbb{U}}(\boldsymbol{\theta})$ indicates the number of achievable DOFs increased from $|\mathbb{S}|$ to $|\mathbb{U}|$ for DOA estimation. Therefore, benefitting from the proposed Nyquist spatial filling in the physical array domain for the generation of a presumed ULA, off-the-shelf Nyquist sampling-based DOA estimation methods can be adopted, such as subspace-based methods [21], sparsity-based methods [36], [37], and their variants [38], [39], [40]. For instance, the multiple signal classification (MUSIC) spatial spectrum corresponding to the presumed ULA $\mathbb{U}$ is given as

$$P_{\mathrm{MUSIC}}(\theta) = \left(\boldsymbol{a}_{\mathbb{U}}^{\mathrm{H}}(\theta)\boldsymbol{E}_n\boldsymbol{E}_n^{\mathrm{H}}\boldsymbol{a}_{\mathbb{U}}(\theta)\right)^{-1}, \tag{18}$$

where $\boldsymbol{E}_n \in \mathbb{C}^{|\mathbb{U}|\times(|\mathbb{U}|-K)}$ spans the noise subspace of the optimized covariance matrix $\boldsymbol{R}_{\boldsymbol{yy}}^{\star}$ corresponding to $\mathbb{U}$. By collecting the directions corresponding to the largest K spectrum responses, the DOAs are estimated as $\hat{\boldsymbol{\theta}} = [\hat{\theta}_1, \hat{\theta}_2, \ldots, \hat{\theta}_K]^{\mathrm{T}}$.

The proposed DOA estimation algorithm via structured correlation reconstruction is summarized in **Algorithm 1**. The computational complexity of solving the proposed optimization problem (17) is $\mathcal{O}(|\mathbb{U}|^{4.5})$ [41], which relates to the array aperture. It is worth highlighting that the proposed algorithm does not incorporate the predefined spatial sampling grids into the optimization problem. Hence, the estimation accuracy will not be limited by the grid density, ensuring the capability of resolving off-grid sources.

Fig. 2. Illustration of the principle difference on the augmented covariance matrix to be retrieved. (a) Virtual array interpolation; (b) Proposed Nyquist spatial filling.

IV. Performance Anylysis

In this section, the performance of the proposed structured correlation reconstruction-based DOA estimation algorithm is analyzed theoretically. First, the relationship between the proposed Nyquist spatial filling approach and the virtual array interpolation-based approaches is established. Then, the Cramér-Rao bound tailored for the proposed DOA estimation problem is derived.

A. Relationship With Virtual Array Interpolation Approaches

The idea of virtual array interpolation had been proposed to address the information loss caused by the discontiguous virtual array, which enables the full utilization of virtual signals for sparse array DOA estimation. For the sake of clarity, here we briefly review the virtual array interpolation-based approaches.

The virtual array signals are obtained by vectorizing the sparse array covariance matrix $\boldsymbol{R}_{\boldsymbol{xx}}$ (3) as

$$\boldsymbol{r}_{\boldsymbol{x}} = \mathrm{vec}\left(\boldsymbol{R}_{\boldsymbol{xx}}\right) = \sum_{k=1}^{K} \sigma_k^2 \boldsymbol{a}_{\mathbb{S}}(\theta_k) \otimes \boldsymbol{a}_{\mathbb{S}}^{\mathrm{H}}(\theta_k) + \sigma_n^2 \mathrm{vec}\left(\boldsymbol{I}\right), \tag{19}$$

whose corresponding virtual array geometry is given as

$$\mathbb{D} = \{u_i d - u_j d, \ \forall u_i d, u_j d \in \mathbb{S}\}. \tag{20}$$

The virtual array $\mathbb{D}$ is contiguous for a fully augmentable array (e.g., nested array), but discontiguous for a partially augmentable array (e.g., coprime array). Therefore, the virtual array interpolation is only applicable for the partially augmentable array to form a virtual ULA $\mathbb{V}$ containing all discontiguous virtual sensors in $\mathbb{D}_+$. Accordingly, the covariance matrix of the interpolated virtual ULA, $\hat{\boldsymbol{R}}_{\boldsymbol{v}}$, can be constructed by rearranging the correlations in $\hat{\boldsymbol{r}}_{\boldsymbol{x}} = \mathrm{vec}(\hat{\boldsymbol{R}}_{\boldsymbol{xx}})$ into a Hermitian Toeplitz matrix, i.e., the diagonals corresponding to the virtual sensors in $\mathbb{D}_+$ are selected from the corresponding entries in $\hat{\boldsymbol{r}}_{\boldsymbol{x}}$, whereas the diagonals corresponding to the interpolated virtual sensors in $\mathbb{V} - \mathbb{D}_+$ are initialized to zeros.

The principle difference between the virtual array interpolation and the proposed Nyquist spatial filling is illustrated in Fig. 2. In particular, for the virtual array interpolation, the discontiguous virtual sensors cause the diagonals of missing elements in the corresponding positions of the augmented covariance matrix $\hat{\boldsymbol{R}}_{\boldsymbol{v}}$. While the main diagonal of $\hat{\boldsymbol{R}}_{\boldsymbol{v}}$ contains the auto-correlations, its strong incoherence property is always satisfied. By contrast, the augmented covariance matrix resulting from Nyquist spatial filling, $\tilde{\boldsymbol{R}}_{\boldsymbol{yy}}$, presents whole rows and columns of missing elements, which makes the matrix completion principle not work.

To interpolate the discontiguous virtual arrays, the matrix completion principle can be utilized to retrieve the unknown correlations in $\hat{\boldsymbol{R}}_{\boldsymbol{v}}$ as [24]

$$\begin{aligned} \min_{\mathrm{Toep}(\boldsymbol{z})\in\mathbb{C}^{|\mathbb{V}|\times|\mathbb{V}|}} \quad & \|\mathrm{Toep}(\boldsymbol{z})\|_* \\ \text{subject to} \quad & \mathcal{P}_\Omega\left(\mathrm{Toep}(\boldsymbol{z})\right) = \mathcal{P}_\Omega(\hat{\boldsymbol{R}}_{\boldsymbol{v}}), \end{aligned} \tag{21}$$

where the equality constraint keeps the observed correlations in $\hat{\boldsymbol{R}}_{\boldsymbol{v}}$ same in the optimized covariance matrix.

More recently, the matrix reconstruction principle has been introduced to reconstruct the covariance matrix corresponding to the interpolated virtual ULA as [26]

$$\begin{aligned} \min_{\mathrm{Toep}(\boldsymbol{z})\in\mathbb{C}^{|\mathbb{V}|\times|\mathbb{V}|}} \quad & \mathrm{Tr}\left(\mathrm{Toep}(\boldsymbol{z})\right) \\ \text{subject to} \quad & \left\|\mathcal{P}_\Omega\left(\mathrm{Toep}(\boldsymbol{z})\right) - \hat{\boldsymbol{R}}_{\boldsymbol{v}}\right\|_F^2 \le \xi, \\ & \mathrm{Toep}(\boldsymbol{z}) \succeq \boldsymbol{0}, \end{aligned} \tag{22}$$

where the inequality constraint enforces the norm of reconstruction error on the observed positions to be bounded by a small threshold $\xi > 0$, and the curled inequality constraint indicates a PSD matrix. The optimized covariance matrix $\mathrm{Toep}(\boldsymbol{z}^\star)$ from (21) or (22) behaves like the covariance matrix of the interpolated virtual ULA $\mathbb{V}$, which thus enables a Nyquist sampling-based DOA estimation in the virtual domain.

By comparing the virtual array interpolation-based optimization problems (21) and (22) with the proposed Nyquist spatial filling-based optimization problem (17), we can establish the following Property to reveal their relationship with respect to DOA estimation performance.

Property 1: There is no DOA estimation performance difference between using the Nyquist spatial filling and the virtual array interpolation, if and only if all the correlations in $\boldsymbol{R}_{\boldsymbol{xx}}$ (11) are included in the reference matrices $\hat{\boldsymbol{R}}_{\boldsymbol{xx}}$ of (17) and $\hat{\boldsymbol{R}}_{\boldsymbol{v}}$ of (21) and (22). □

Proof: In order to validate the claimed property, we analyze the above-mentioned approaches from three aspects, namely, retrieved covariance matrix, nuclear norm penalty, and the correlation fitting component.

Retrieved Covariance Matrix: In the framework of virtual array interpolation, the correlations in the covariance matrix $\mathrm{Toep}(\boldsymbol{z}^\star) \in \mathbb{C}^{|\mathbb{V}|\times|\mathbb{V}|}$ optimized by the matrix completion principle remain the same as the observed correlations in $\hat{\boldsymbol{R}}_{\boldsymbol{v}}$ that correspond to the discontiguous virtual array $\mathbb{D}_+$, whereas the optimization problem (22) using the matrix reconstruction principle forms a denoising constraint to minimize the difference between the observed correlations in $\hat{\boldsymbol{R}}_{\boldsymbol{v}}$ and those in the corresponding positions of $\mathrm{Toep}(\boldsymbol{z}^\star)$. Here, the interpolation in the virtual domain indicates that $|\mathbb{V}| = \max(\mathbb{D}_+) + 1$. On the other hand, the incorporation of the sketching matrix $\boldsymbol{\Phi}$ in the proposed Nyquist spatial filling-based approach (17) directly takes the sample covariance matrix $\hat{\boldsymbol{R}}_{\boldsymbol{xx}}$ as the reference for denoising. Meanwhile, the *prior* information on the matrix structure is required for retrieving the unknown entries in the whole rows and columns of the $|\mathbb{U}|\times|\mathbb{U}|$ dimensional augmented covariance matrix corresponding to the presumed ULA. According to the procedure of Nyquist spatial filling of a physical array in Section III-A, we have $|\mathbb{U}| = \max(\mathbb{S}) + 1$. From (20), we have $\max(\mathbb{D}_+) = \max(\mathbb{S})$, and hence the relationship

$$|\mathbb{V}| = \max(\mathbb{D}_+) + 1 = \max(\mathbb{S}) + 1 = |\mathbb{U}| \tag{23}$$

holds. While all above-mentioned optimization problems (17), (21) and (22) enforce the optimized matrix a Hermitian Toeplitz structure, both the retrieved covariance matrix $\boldsymbol{R}^\star_{\boldsymbol{yy}} \in \mathbb{C}^{|\mathbb{U}|\times|\mathbb{U}|}$ from the proposed Nyquist spatial filling and those optimized from the virtual array interpolation, i.e., $\mathrm{Toep}(\boldsymbol{z}^\star) \in \mathbb{C}^{|\mathbb{V}|\times|\mathbb{V}|}$, have the same matrix dimension. Hence, the subsequently incorporated Nyquist sampling-based DOA estimation methods operate with a similarly structured ULA. ■

Nuclear Norm Penalty: As the convex envelope of the rank function, the nuclear norm is incorporated into the formulated optimization problems (17) and (21), representing an approximation to the upper-bound of the matrix rank. Although the virtual domain atomic norm is applied for gridless reconstruction with atomic norm minimization in [26], its objective function is eventually cast as a trace minimization problem in (22) according to the properties of the atomic norm for multiple virtual measurements. Note that, both optimization problems (17) and (22) claim a PSD constraint on the optimized covariance matrix, i.e., $\lambda_u(\boldsymbol{R}^\star_{\boldsymbol{yy}}) \ge 0, u = 1, 2, \ldots, |\mathbb{U}|$ and $\lambda_v(\mathrm{Toep}(\boldsymbol{z}^\star)) \ge 0, v = 1, 2, \ldots, |\mathbb{V}|$. While $\boldsymbol{R}^\star_{\boldsymbol{yy}}$ and $\mathrm{Toep}(\boldsymbol{z}^\star)$ are square matrices, it is obvious that

$$\left\|\boldsymbol{R}^\star_{\boldsymbol{yy}}\right\|_* = \sum_{u=1}^{|\mathbb{U}|} \lambda_u\left(\boldsymbol{R}^\star_{\boldsymbol{yy}}\right) = \mathrm{Tr}\left(\boldsymbol{R}^\star_{\boldsymbol{yy}}\right), \tag{24}$$

$$\left\|\mathrm{Toep}(\boldsymbol{z}^\star)\right\|_* = \sum_{v=1}^{|\mathbb{V}|} \lambda_v\left(\mathrm{Toep}(\boldsymbol{z}^\star)\right) = \mathrm{Tr}\left(\mathrm{Toep}(\boldsymbol{z}^\star)\right), \tag{25}$$

indicating an equivalence relationship between the trace operator and the nuclear norm operator in the considered optimization problems. Therefore, the nuclear norm penalty in the proposed optimization problem (17) has the same effect as the objective functions of both virtual array interpolation-based optimization problems (21) and (22). While the nuclear norm or trace norm is the convex envelope of the matrix rank for convex relaxation, it has been pointed out in [42] that the original rank penalty term can be further approximated by applying a family of non-convex penalties, where the suboptimal solution is capable of approaching the theoretical one. ■

Correlation Fitting Component: In the virtual array interpolation-based approaches, the correlations in $\hat{\boldsymbol{R}}_{\boldsymbol{v}}$ corresponding to the discontiguous virtual sensors in $\mathbb{D}_+$ can be selected from $\hat{\boldsymbol{r}}_{\boldsymbol{x}}$ corresponding to their respective lags. It has been revealed in [43] that

$$\mathrm{E}\left[\hat{\boldsymbol{r}}_{\boldsymbol{x}}\hat{\boldsymbol{r}}_{\boldsymbol{x}}^{\mathrm{H}}\right] = \boldsymbol{r}_{\boldsymbol{x}}\boldsymbol{r}_{\boldsymbol{x}}^{\mathrm{H}} + \frac{1}{L}\left(\boldsymbol{R}_{\boldsymbol{xx}}^{\mathrm{T}} \otimes \boldsymbol{R}_{\boldsymbol{xx}}\right), \tag{26}$$

indicating that the vectorized sample covariance matrix $\hat{\boldsymbol{r}}_{\boldsymbol{x}}$ calculated from finite snapshots contains multiple entries corresponding to the same lag. While different pairs of elements in $\mathbb{S}$ may correspond to the same virtual sensor in $\mathbb{D}$ according to (20), not all the correlations in $\hat{\boldsymbol{R}}_{\boldsymbol{xx}}$ are effectively utilized with such a selection. Alternatively, by replacing the selection process with an averaging process, where the correlations corresponding to the same lag in $\hat{\boldsymbol{R}}_{\boldsymbol{xx}}$ are averaged to form $\hat{\boldsymbol{R}}_{\boldsymbol{v}}$, the virtual array interpolation-based approaches are capable of taking all the available information as the proposed Nyquist spatial filling-based approach. With such an average, they share the same information from the reference matrix $\hat{\boldsymbol{R}}_{\boldsymbol{xx}}$ or $\hat{\boldsymbol{R}}_{\boldsymbol{v}}$ for optimizing the augmented covariance matrix. Furthermore, according to the conclusions drawn in [22], a performance closer to the CRB can be obtained by properly sampling the correlations from the sample covariance matrix $\hat{\boldsymbol{r}}_{\boldsymbol{x}}$ with a certain strategy instead of simply performing an average. ■

While it is clear from (26) that $\hat{\boldsymbol{r}}_{\boldsymbol{x}}$ tends to $\boldsymbol{r}_{\boldsymbol{x}}$ when the number of snapshots L goes to infinity, we can conclude that on the premise of utilizing all the correlations in the ideal $\boldsymbol{R}_{\boldsymbol{xx}}$ for the optimization, the virtual array interpolation-based approaches have the same DOA estimation performance as the proposed algorithm, where the Property 1 is validated. Nevertheless, owing to the incorporation of the sketching matrix $\boldsymbol{\Phi}$ relating $\mathbb{S}$ and $\mathbb{U}$, the proposed algorithm is more flexible to cope with a general class of sparse array configurations without investigating the characteristic of derived virtual array, and the structured correlation reconstruction ensures an effective retrieval of the augmented covariance matrix resulting from Nyquist spatial filling in the physical array domain.

B. The Cramér-Rao Bound

As a lower bound on the variance of any unbiased estimator, the Cramér-Rao bound can be utilized as a unified metric for evaluating the performance of parameter estimation. For the unconditional model as defined in (1), the lower bound of the DOA estimation performance can be represented by the stochastic CRB, which is calculated from the inversion of the Fisher information matrix [44]. However, when the number of sources exceeds the number of physical sensors, its Fisher information matrix becomes singular, rendering the stochastic CRB invalid. In this subsection, we derive the CRB tailored for the proposed structured correlation reconstruction-based DOA estimation with Nyquist spatial filling, where both the overdetermined case ($K < |\mathbb{S}|$) and the underdetermined case ($K \geq |\mathbb{S}|$) are included.

For the proposed algorithm, the DOA estimation is accomplished in the processing of the reconstructed covariance matrix $\boldsymbol{R}^{\star}_{\boldsymbol{yy}}$, which has an augmented dimension of $|\mathbb{U}| \times |\mathbb{U}|$ corresponding to the presumed ULA $\mathbb{U}$. Nevertheless, from the information perspective, only the observed correlations calculated from the received signals $\boldsymbol{x}(l)$ of the sparse array $\mathbb{S}$ are effective, reflected by the non-zero entries in the augmented covariance matrix $\tilde{\boldsymbol{R}}_{\boldsymbol{yy}}$. Although the unknown correlations represented as zeros in $\tilde{\boldsymbol{R}}_{\boldsymbol{yy}}$ have been retrieved from the optimization problem (17), the effective information beyond the correlations contained in $\hat{\boldsymbol{R}}_{\boldsymbol{xx}}$ is not increased. Therefore, the (m, n)-th entry in the Fisher information matrix $\boldsymbol{F}$ can be calculated from $\boldsymbol{R}_{\boldsymbol{xx}}$ as [44], [45], [46]

$$\boldsymbol{F}_{m,n} = L\,\mathrm{Tr}\left[\boldsymbol{R}^{-1}_{\boldsymbol{xx}}\frac{\partial \boldsymbol{R}_{\boldsymbol{xx}}}{\partial \beta_m}\boldsymbol{R}^{-1}_{\boldsymbol{xx}}\frac{\partial \boldsymbol{R}_{\boldsymbol{xx}}}{\partial \beta_n}\right], \tag{27}$$

where β_m and β_n denote the m-th and n-th entry of the parameter vector $\boldsymbol{\beta}$, respectively. For the DOA estimation problem, the unknown parameters include the DOAs of sources $\boldsymbol{\theta}$ and their power $\boldsymbol{p}$, as well as the noise power σ_n^2. As such, the parameter vector $\boldsymbol{\beta}$ can be expressed as

$$\boldsymbol{\beta} = \left[\boldsymbol{\theta}^{\mathrm{T}}, \boldsymbol{p}^{\mathrm{T}}, \sigma_n^2\right]^{\mathrm{T}}. \tag{28}$$

While the DOAs are estimated from the augmented covariance matrix $\boldsymbol{R}_{\boldsymbol{yy}}$ to achieve an increased number of DOFs, according to the compressed transformation relationship established in (11), the Fisher information matrix $\boldsymbol{F}$ in (27) can be calculated with respect to the theoretical covariance matrix of the presumed ULA $\boldsymbol{R}_{\boldsymbol{yy}}$ and the sketching matrix $\boldsymbol{\Phi}$ as

$$\boldsymbol{F}_{m,n} = L\,\mathrm{Tr}\left[\boldsymbol{R}^{-1}_{\boldsymbol{xx}}\frac{\partial\left(\boldsymbol{\Phi}\boldsymbol{R}_{\boldsymbol{yy}}\boldsymbol{\Phi}^{\mathrm{T}}\right)}{\partial \beta_m}\boldsymbol{R}^{-1}_{\boldsymbol{xx}}\frac{\partial\left(\boldsymbol{\Phi}\boldsymbol{R}_{\boldsymbol{yy}}\boldsymbol{\Phi}^{\mathrm{T}}\right)}{\partial \beta_n}\right], \tag{29}$$

where the partial derivative operation is related to $\boldsymbol{R}_{\boldsymbol{yy}}$ because the sketching matrix $\boldsymbol{\Phi}$ only depends on the array configurations and is independent of any parameter in $\boldsymbol{\beta}$. According to the property of the trace operator, we have $\mathrm{Tr}(\boldsymbol{ABCD}) = [\mathrm{vec}(\boldsymbol{B}^{\mathrm{H}})]^{\mathrm{H}}(\boldsymbol{A}^{\mathrm{T}} \otimes \boldsymbol{C})\mathrm{vec}(\boldsymbol{D})$. In addition, while $\boldsymbol{R}_{\boldsymbol{xx}}$ is non-singular, we have $(\boldsymbol{R}_{\boldsymbol{xx}} \otimes \boldsymbol{R}_{\boldsymbol{xx}})^{-1} = \boldsymbol{R}^{-1}_{\boldsymbol{xx}} \otimes \boldsymbol{R}^{-1}_{\boldsymbol{xx}}$. Then, the derivation process of the Fisher information matrix continues as

$$\boldsymbol{F}_{m,n} = L\left[\mathrm{vec}\left(\frac{\partial\left(\boldsymbol{\Phi}\boldsymbol{R}_{\boldsymbol{yy}}\boldsymbol{\Phi}^{\mathrm{T}}\right)}{\partial \beta_m}\right)\right]^{\mathrm{H}}\left(\boldsymbol{R}^{\mathrm{T}}_{\boldsymbol{xx}} \otimes \boldsymbol{R}_{\boldsymbol{xx}}\right)^{-1} \mathrm{vec}\left(\frac{\partial\left(\boldsymbol{\Phi}\boldsymbol{R}_{\boldsymbol{yy}}\boldsymbol{\Phi}^{\mathrm{T}}\right)}{\partial \beta_n}\right). \tag{30}$$

Combining the equivalent transformation of the vectorization process, i.e., $\mathrm{vec}(\boldsymbol{\Phi}\boldsymbol{R}_{\boldsymbol{yy}}\boldsymbol{\Phi}^{\mathrm{T}}) = (\boldsymbol{\Phi} \otimes \boldsymbol{\Phi})\mathrm{vec}(\boldsymbol{R}_{\boldsymbol{yy}})$, the Fisher information matrix can be further represented as

$$\boldsymbol{F} = L\left[\frac{\mathrm{vec}\left(\partial \boldsymbol{R}_{\boldsymbol{yy}}\right)}{\partial \boldsymbol{\beta}}\right]^{\mathrm{H}}(\boldsymbol{\Phi} \otimes \boldsymbol{\Phi})^{\mathrm{T}}\left(\boldsymbol{R}^{\mathrm{T}}_{\boldsymbol{xx}} \otimes \boldsymbol{R}_{\boldsymbol{xx}}\right)^{-1} (\boldsymbol{\Phi} \otimes \boldsymbol{\Phi})\frac{\mathrm{vec}\left(\partial \boldsymbol{R}_{\boldsymbol{yy}}\right)}{\partial \boldsymbol{\beta}}. \tag{31}$$

By incorporating the property for the Kronecker product calculation $(\boldsymbol{A} \otimes \boldsymbol{B})(\boldsymbol{C} \otimes \boldsymbol{D}) = \boldsymbol{AC} \otimes \boldsymbol{BD}$, the Fisher information matrix can be further calculated as.

$$\begin{aligned}\boldsymbol{F} &= L\left[\frac{\mathrm{vec}\left(\partial \boldsymbol{R}_{\boldsymbol{yy}}\right)}{\partial \boldsymbol{\beta}}\right]^{\mathrm{H}}\left(\left(\boldsymbol{R}^{-1}_{\boldsymbol{xx}}\boldsymbol{\Phi}\right)^{\mathrm{T}} \otimes \left(\boldsymbol{\Phi}^{\mathrm{T}}\boldsymbol{R}^{-1}_{\boldsymbol{xx}}\right)\right)(\boldsymbol{\Phi} \otimes \boldsymbol{\Phi})\frac{\mathrm{vec}\left(\partial \boldsymbol{R}_{\boldsymbol{yy}}\right)}{\partial \boldsymbol{\beta}}\\ &= L\left[\frac{\mathrm{vec}\left(\partial \boldsymbol{R}_{\boldsymbol{yy}}\right)}{\partial \boldsymbol{\beta}}\right]^{\mathrm{H}}\left(\left(\boldsymbol{\Phi}^{\mathrm{T}}\boldsymbol{R}^{-1}_{\boldsymbol{xx}}\boldsymbol{\Phi}\right)^{\mathrm{T}} \otimes \left(\boldsymbol{\Phi}^{\mathrm{T}}\boldsymbol{R}^{-1}_{\boldsymbol{xx}}\boldsymbol{\Phi}\right)\right)\frac{\mathrm{vec}\left(\partial \boldsymbol{R}_{\boldsymbol{yy}}\right)}{\partial \boldsymbol{\beta}}.\end{aligned} \tag{32}$$

According to the compressed transformation relationship between $\boldsymbol{R}_{\boldsymbol{xx}}$ and $\boldsymbol{R}_{\boldsymbol{yy}}$ as established in (11), the Fisher information matrix can be finally represented only related to the theoretical covariance matrix of the presumed ULA $\boldsymbol{R}_{\boldsymbol{yy}}$ as in (33) shown at the bottom of the next page. Considering that the sketching matrix $\boldsymbol{\Phi}$ is a non-square and singular matrix, the term $(\boldsymbol{\Phi}\boldsymbol{R}_{\boldsymbol{yy}}\boldsymbol{\Phi}^{\mathrm{H}})^{-1}$ cannot be further decomposed. The

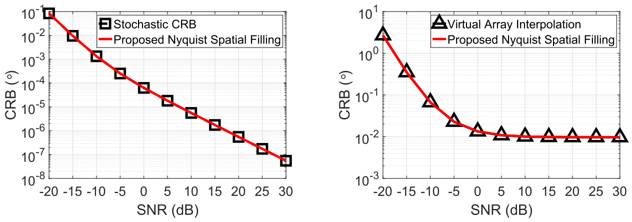

(a) (b)

Fig. 3. Comparison of the Cramér-Rao bounds. (a) Overdetermined case; (b) Underdetermined case.

above-mentioned derivation on Fisher information matrix from (29) to (33) effectively reflects the compressed transformation relationship established by $\boldsymbol{\Phi}$.

According to the definition of $\boldsymbol{R_{yy}}$ in (12), its vectorization follows

$$\begin{aligned} \boldsymbol{r_y} &= \text{vec}\left(\boldsymbol{R_{yy}}\right) = \left(\boldsymbol{A}^*_{\mathbb{U}}(\boldsymbol{\theta}) \odot \boldsymbol{A}_{\mathbb{U}}(\boldsymbol{\theta})\right)\boldsymbol{p} + \sigma_n^2 \boldsymbol{i}_{|\mathbb{U}|}, \\ &= \sum_{k=1}^{K} \sigma_k^2 \boldsymbol{a}^*_{\mathbb{U}}(\theta_k) \otimes \boldsymbol{a}_{\mathbb{U}}(\theta_k) + \sigma_n^2 \boldsymbol{i}_{|\mathbb{U}|}, \end{aligned} \tag{34}$$

where $\boldsymbol{i}_{|\mathbb{U}|} \in \mathbb{R}^{|\mathbb{U}|^2}$ denotes the vectorization of the $|\mathbb{U}| \times |\mathbb{U}|$ dimensional identity matrix. Then, the vectorized form of the partial derivative of $\boldsymbol{R_{yy}}$ with respect to $\boldsymbol{\beta}$ becomes

$$\frac{\text{vec}\left(\partial \boldsymbol{R_{yy}}\right)}{\partial \boldsymbol{\beta}} = \frac{\partial \boldsymbol{r_y}}{\partial \boldsymbol{\beta}} = \left[\frac{\partial \boldsymbol{r_y}}{\partial \boldsymbol{\theta}}, \frac{\partial \boldsymbol{r_y}}{\partial \boldsymbol{p}}, \frac{\partial \boldsymbol{r_y}}{\partial \sigma_n^2}\right], \tag{35}$$

where

$$\frac{\partial \boldsymbol{r_y}}{\partial \boldsymbol{\theta}} = \left(\frac{\partial \boldsymbol{A}^*_{\mathbb{U}}(\boldsymbol{\theta})}{\partial \boldsymbol{\theta}} \odot \boldsymbol{A}_{\mathbb{U}}(\boldsymbol{\theta}) + \boldsymbol{A}^*_{\mathbb{U}}(\boldsymbol{\theta}) \odot \frac{\partial \boldsymbol{A}_{\mathbb{U}}(\boldsymbol{\theta})}{\partial \boldsymbol{\theta}}\right)\boldsymbol{P}, \tag{36}$$

$$\frac{\partial \boldsymbol{r_y}}{\partial \boldsymbol{p}} = \boldsymbol{A}^*_{\mathbb{U}}(\boldsymbol{\theta}) \odot \boldsymbol{A}_{\mathbb{U}}(\boldsymbol{\theta}), \tag{37}$$

$$\frac{\partial \boldsymbol{r_y}}{\partial \sigma_n^2} = \boldsymbol{i}_{|\mathbb{U}|}. \tag{38}$$

Then, the CRB for the proposed DOA estimation algorithm is the inverse of the Fisher information matrix as

$$\text{CRB}(\boldsymbol{\beta}) = \boldsymbol{F}^{-1}, \tag{39}$$

which is feasible to indicate the performance bound of DOA estimation in both overdetermined and underdetermined cases.

We compare the Cramér-Rao bounds for estimating the DOAs in Fig. 3 with Nyquist spatial filling in both the virtual array domain and the proposed physical array domain, where the sparse array consists of 7 physical sensors located at 0, $3d$, $5d$, $6d$, $9d$, $10d$, and $12d$, respectively. In the overdetermined case, we consider a single random source from $\mathcal{N}(0^\circ, 1^\circ)$, whose direction changes from trial to trial but remains fixed from snapshot to snapshot. In the underdetermined case, we consider 10 sources uniformly distributed in $[-60^\circ, 60^\circ]$. The number of snapshots is 500, and the CRB is averaged over 500 Monte-Carlo trials. According to Fig. 3(a), the CRB for the proposed algorithm, (39), overlaps with the stochastic CRB, indicating that the derived CRB degenerates to the conventional stochastic CRB when $K < |\mathbb{S}|$. While the stochastic CRB does not exist when $K \geq |\mathbb{S}|$, we compare the CRB for the virtual array interpolation-based DOA estimation approach [26] and the derived CRB for the Nyquist spatial filling-based DOA estimation (39). It is clear from Fig. 3(b) that both CRBs present the same response when the signal-to-noise ratio (SNR) varies. Hence, the performance lower bound for DOA estimation is determined by the correlations in the ideal sparse array covariance matrix $\boldsymbol{R_{xx}}$ as in (3), regardless of the subsequent operation either in the physical array domain or in the virtual array domain. The observation from this CRB comparison further validates the equivalence revealed in Property 1 in a theoretical manner.

It is worth noting that the Cramér-Rao bound is typically tight asymptotically. The most recent work on performance bound analysis derived an explicit Ziv-Zakai bound for both overdetermined DOAs estimation and underdetermined DOAs estimation [47], which is global tight to evaluate the estimation performance especially in the low SNR regime.

V. Simulation Results

In this section, we present simulation results to demonstrate the performance of the proposed DOA estimation algorithm. A coprime array configuration, which belongs to a partially augmentable array with a systematic design, is first considered for performance comparison. Then, different sparse array configurations are adopted to illustrate the effectiveness of the proposed algorithm.

A. Achievable DOFs

We consider a coprime array composed of 7 sensors locating at $\mathbb{S}_{\text{coprime}} = \{0, 3d, 5d, 6d, 9d, 10d, 12d\}$. To indicate the increased number of DOFs, the underdetermined case with 9 sources is considered. The proposed structured correlation reconstruction-based algorithm is compared to two coprime array DOA estimation algorithms, namely, the covariance matrix sparse reconstruction (CMSR) algorithm [16] and the sparse signal reconstruction (SSR) algorithm [37]. Meanwhile, the Capon algorithm operating on an ULA consisting of the same 7 physical sensors is also presented for reference. The regularization parameter for the proposed algorithm is $\mu = 2.5 \times 10^{-3}$, which is heuristically selected according to the simulation parameter setting as well as the practical experience. The normalized spectra of the tested algorithms are depicted in Fig. 4, where the SNR is set to 0 dB and the number of snapshots $L = 500$. The red vertical dashed lines in each spectrum represent the true DOAs.

Since the ULA consisting of 7 sensors can only distinguish at most 6 sources, the Capon spectrum shown in Fig. 4(a) fails to resolve all 9 sources. Although exploiting the coprime array breaks through the DOFs limitation constrained by the

$$\boldsymbol{F} = L\left[\frac{\text{vec}\left(\partial \boldsymbol{R_{yy}}\right)}{\partial \boldsymbol{\beta}}\right]^{\text{H}} \left\{\left[\boldsymbol{\Phi}^{\text{T}}\left(\boldsymbol{\Phi}\boldsymbol{R_{yy}}\boldsymbol{\Phi}^{\text{H}}\right)^{-1}\boldsymbol{\Phi}\right]^{\text{T}} \otimes \left[\boldsymbol{\Phi}^{\text{T}}\left(\boldsymbol{\Phi}\boldsymbol{R_{yy}}\boldsymbol{\Phi}^{\text{H}}\right)^{-1}\boldsymbol{\Phi}\right]\right\} \frac{\text{vec}\left(\partial \boldsymbol{R_{yy}}\right)}{\partial \boldsymbol{\beta}}. \tag{33}$$

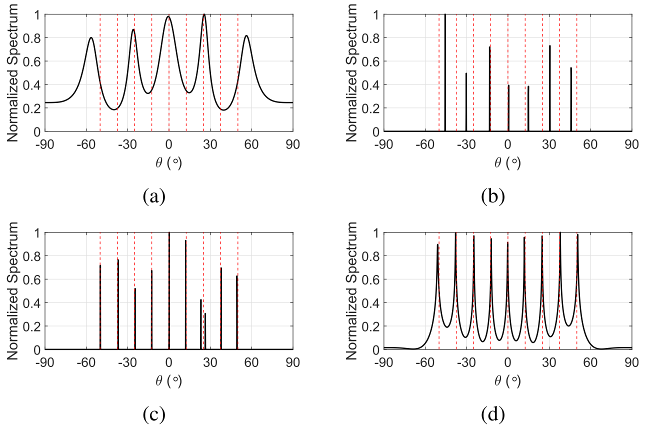

Fig. 4. Normalized spectrum comparison with 9 sources. (a) Capon algorithm using ULA; (b) CMSR algorithm; (c) SSR algorithm; (d) Proposed algorithm.

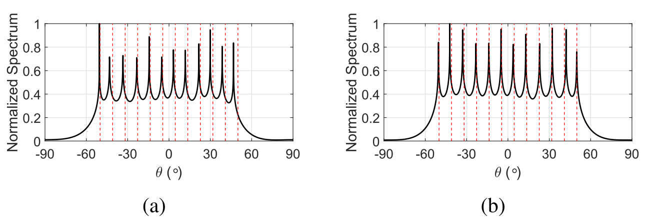

Fig. 5. Normalized spectrum comparison with 12 sources. (a) Virtual array interpolation algorithm; (b) Proposed Nyquist spatial filling algorithm.

number of physical sensors, the CMSR algorithm only utilizes the contiguous segment of the discontiguous virtual array $\mathbb{V}_{\text{coprime}} = \{-12d, -10d, -9d, -7d, \ldots, 7d, 9d, 10d, 12d\}$ for virtual domain signal processing. Therefore, the maximum achievable DOFs for the CMSR algorithm is 7, accounting for the failure of source identification presented in Fig. 4(b). While the SSR algorithm makes full use of the discontiguous virtual array $\mathbb{V}_{\text{coprime}}$, it is capable of identifying all the 9 sources, as shown in Fig. 4(c). Nevertheless, there exist several spurious peaks in the spatial spectrum, which is caused by the suboptimal solution to its relaxed sparsity constraint. In contrast, the proposed algorithm presents the best spectrum characteristic among all tested algorithms in Fig. 4, since it makes full use of the sparse array received signals while maintaining an ULA-based signal processing for DOA estimation.

While the optimized covariance matrix $\boldsymbol{R}_{\boldsymbol{yy}}^{\star}$ corresponds to the presumed ULA with 13 sensors ranging from 0 to $12d$, we increase the number of sources to $K = 12$ to evaluate its maximum achievable DOFs. In Fig. 5, the proposed Nyquist spatial filling-based algorithm is compared with the virtual array interpolation algorithm [26]. It is clear from Fig. 5(b) that the proposed algorithm successfully identifies all the 12 sources with 7 physical sensors, indicating that the Nyquist spatial filling and the associated structured correlation reconstruction enable a larger number of DOFs than the discontiguous virtual array $\mathbb{V}_{\text{coprime}}$. Although performing virtual array interpolation can also present 12 response peaks in the spectrum, due to the selection of the virtual domain correlations that correspond to the same lag, several peaks apparently deviate from the true directions as shown in Fig. 5(a).

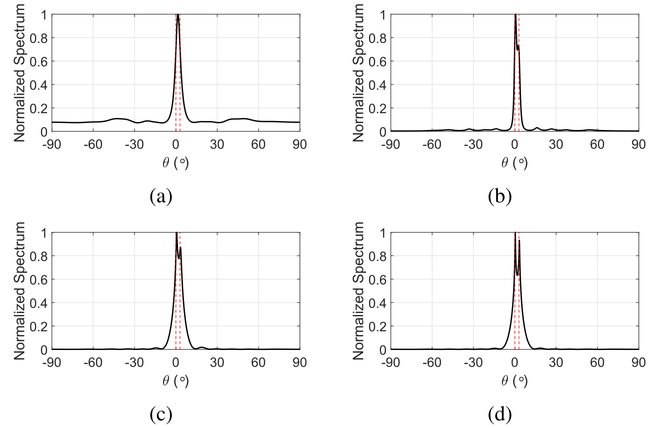

Fig. 6. Resolution comparison. (a) Capon algorithm using coprime array; (b) SSR algorithm; (c) Virtual array interpolation algorithm; (d) Proposed algorithm.

B. Resolution Performance

We then compare the resolution of the proposed algorithm with those of the Capon algorithm, the SSR algorithm, and the virtual array interpolation (VAI) algorithm, where two closely spaced sources impinge from 0° and 5°. In this subsection, all the algorithms are applied on the coprime array $\mathbb{S}_{\text{coprime}}$ with an aperture of $12d$. The SNRs of both sources are set to 0 dB, and the number of snapshots is $L = 500$.

The normalized spectra of the tested algorithms are compared in Fig. 6. Although the Capon algorithm incorporates the same coprime array as other algorithms, it fails to identify the two sources as shown in Fig. 6(a). The spectrum characteristic of the SSR algorithm directly operating on the entire discontiguous virtual array is not satisfactory, where one peak is not quite obvious as shown in Fig. 6(b). In contrast, both the virtual array interpolation algorithm and the proposed Nyquist spatial filling-based algorithm are capable of distinguishing these two closely-spaced sources, and the proposed algorithm shows sharper response peaks than the virtual array interpolation algorithm. The comparison result indicates that the proposed algorithm owns a more reliable performance than the virtual array interpolation algorithm in the matrix reconstruction process.

To further demonstrate the angular resolution of the proposed algorithm, we compare the identification rate by varying the interval between the two sources. In particular, assume that the first source θ_1 is randomly generated from a normal distribution $\mathcal{N}(0^\circ, 1^\circ)$, whose direction changes from trial to trial but remains fixed from snapshot to snapshot. Moreover, the second source has the direction $\theta_2 = \theta_1 + \Delta\theta$, where $\Delta\theta$ denotes the directional interval between the two sources. The identification rate is defined as the percentage of success trials among 500 Monte-Carlo trials, where a trial is regarded as successful if $|\theta_1 - \theta_2| < \Delta\theta/2$. To maintain a fair comparison, the interval for spectrum searching or predefined spatial sampling grids in each algorithm is set to 0.1°.

The identification rates of the tested algorithms with respect to the directional interval $\Delta\theta$ are compared in Fig. 7. It is obvious that the Capon algorithm requires the largest interval to achieve the same identification rate as the other algorithms. Although the SSR algorithm and the virtual array interpolation (VAI) algorithm make full use of the discontiguous virtual array, their

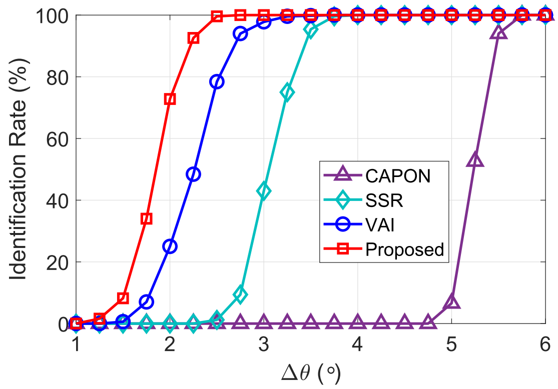

Fig. 7. Identification rate versus directional interval in the case of SNR $= 0$ dB and $L = 500$.

identification rates are inferior to the proposed algorithm. In contrast, by taking advantage of the Nyquist spatial filling and structured correlation reconstruction, the proposed algorithm has the best resolution among the tested algorithms and achieves the full identification rate with a 2.5° directional interval.

C. Estimation Accuracy

To evaluate the estimation accuracy, we compare the root mean square error (RMSE) of the tested DOA estimation algorithms. The RMSE is defined as

$$\mathrm{RMSE} = \sqrt{\frac{1}{KN}\sum_{n=1}^{N}\sum_{k=1}^{K}\left(\hat{\theta}_{k,n} - \theta_k\right)^2}, \tag{40}$$

where $\hat{\theta}_{k,n}$ denotes the estimate of the k-th source θ_k in the n-th Monte-Carlo trial, and $N = 500$ denotes the number of Monte-Carlo trials. In certain trial when the simulated method fails to identify all the sources, i.e., the number of estimated DOAs in $\hat{\boldsymbol{\theta}}$ is less than K, we add additional zeros to meet the RMSE criterion (40), and both the resulting K DOA estimation results and the ideal DOAs $\boldsymbol{\theta}$ are sorted in ascend order for RMSE calculation. Meanwhile, the corresponding CRB (39) is also plotted as a reference.

We first consider the underdetermined case with 9 off-grid sources from the directions $\theta_k = \bar{\theta}_k + \theta_r, k = 1, 2, \ldots, 9$, where $\{\bar{\theta}_k, k = 1, 2, \ldots, 9\}$ are the fixed directions uniformly distributed in $[-50^\circ, 50^\circ]$ while the random term $\theta_r \sim \mathcal{N}(0^\circ, 1^\circ)$ changes from trial to trial but remains fixed from snapshot to snapshot. It is demonstrated in Fig. 8(a) that the proposed algorithm outperforms the virtual array interpolation algorithm, and its RMSE converges to a similar value as that of the SSR algorithm. The reason lies in the fact that the virtual array interpolation algorithm only selects a part of the correlations corresponding to the discontiguous virtual array for reconstructing the covariance matrix of an interpolated ULA. Hence, the information loss is inevitable, since there may exist multiple correlations in the sample covariance matrix $\hat{\boldsymbol{R}}_{\boldsymbol{xx}}$ corresponding to a certain lag/virtual sensor. In contrast, both the proposed algorithm and the SSR algorithm utilize all the correlations in $\hat{\boldsymbol{R}}_{\boldsymbol{xx}}$, which hence lead to a better performance. Nevertheless, the SSR algorithm directly operates on the second-order statistics corresponding to the discontiguous virtual array with a relaxed sparsity constraint, the irregular spurious peaks as illustrated in Fig. 4(c) cause a negative effect on DOA estimation. On the other hand, the structured correlation reconstruction (17) not only enables the proposed algorithm to reconstruct the covariance matrix corresponding to a presumed ULA, but also utilizes all the correlations of the received signals. It is shown in Fig. 8(b) that for a given SNR (10 dB), the proposed algorithm provides a better estimation accuracy regardless of the numbers of snapshots, where the abnormal point in the curve of the SSR algorithm is due to the irregular spurious peaks that appear in its spatial spectrum.

We then compare the DOA estimation accuracy in the maximum achievable DOFs case, where 12 sources uniformly distributed in $[-50^\circ, 50^\circ]$ are simulated. While $K = 12$ exceeds the maximum achievable DOFs offered by the discontiguous virtual array $\mathbb{D}$, only the proposed algorithm and the virtual array interpolation algorithm are compared in Fig. 9. Different from the conventional thinking, in such extreme scenario, the RMSE curve presents a minimal value when the SNR equals to 0 dB and goes relatively flat when SNR is larger than 5 dB. Nevertheless, it is clear from Fig. 9 that the proposed algorithm outperforms the virtual array interpolation algorithm within the entire region we simulated.

We also consider the overdetermined case assuming a single source with the direction randomly generated from $\mathcal{N}(0^\circ, 1^\circ)$ in each Monte-Carlo trial. Different from the underdetermined case where the CRB converges to a constant, it can be inferred from Fig. 3 that the CRB keeps decreasing with the increase of the SNR in the overdetermined case. Hence, to avoid the performance limitation of DOA estimation caused by the fixed spectrum searching interval, the search-free root MUSIC algorithm [48] is used to process the optimized covariance matrices in the proposed algorithm and the virtual array interpolation algorithm. In Fig. 10, the proposed algorithm is compared to the SSR algorithm, the virtual array interpolation algorithm, and the spatial smoothing-based MUSIC (SS-MUSIC) algorithm [21]. While the SSR algorithm and the SS-MUSIC algorithm suffer from a performance limitation caused by either fixed predefined spatial sampling grids or inherent spectrum searching interval, their RMSE curves become relatively flat when the SNR is larger than 5 dB as shown in Fig. 10(a). It is observed that there is a constant gap between the RMSE curve and the CRB for the virtual array interpolation algorithm when the SNR is larger than -10 dB although the trend is consistent with the CRB, whereas the RMSE of the proposed algorithm almost overlaps with the CRB when the SNR is larger than -10 dB. The simulation results in Fig. 10(b) also indicate the superiority of the proposed algorithm compared with other tested algorithms in scenarios with a different number of snapshots.

D. Sparse Array Configurations

To evaluate the performance of the proposed algorithm under different sparse array configurations, we compare the RMSE and the corresponding CRB in Fig. 11 for both the overdetermined case and the underdetermined case. Three sparse array configurations with 7 physical sensors including the minimum redundancy array (MRA), the nested array, and the random array are considered. In particular, the sensors of the MRA and the nested array are respectively located in $\mathbb{S}_{\text{MRA}} = \{0, d, 8d, 11d, 13d, 15d, 17d\}$ and $\mathbb{S}_{\text{nested}} =$

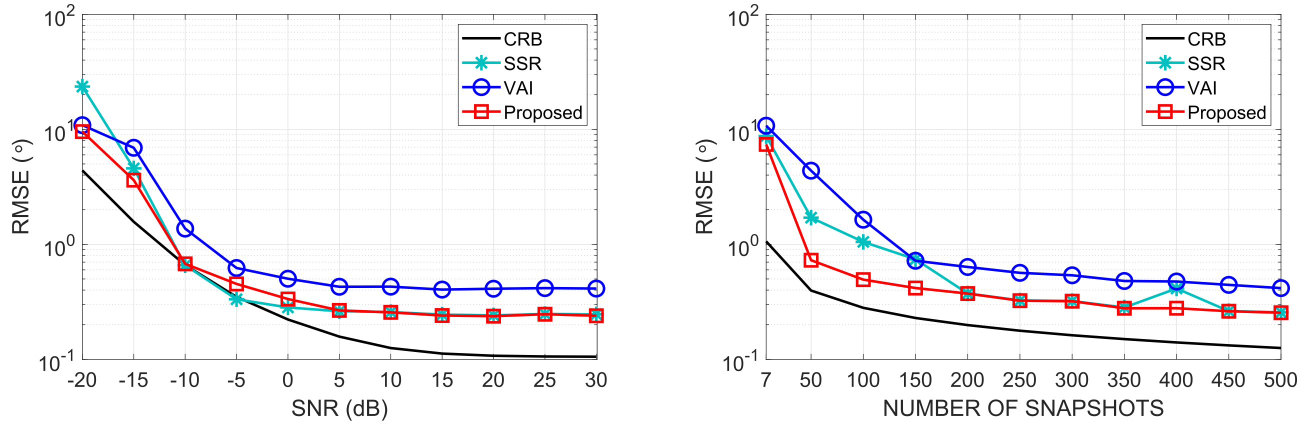

(a) (b)

Fig. 8. DOA estimation accuracy comparison in the underdetermined case with 9 off-grid sources. (a) RMSE versus SNR when the number of snapshots $L = 500$; (b) RMSE versus the number of snapshots when SNR $= 10$ dB.

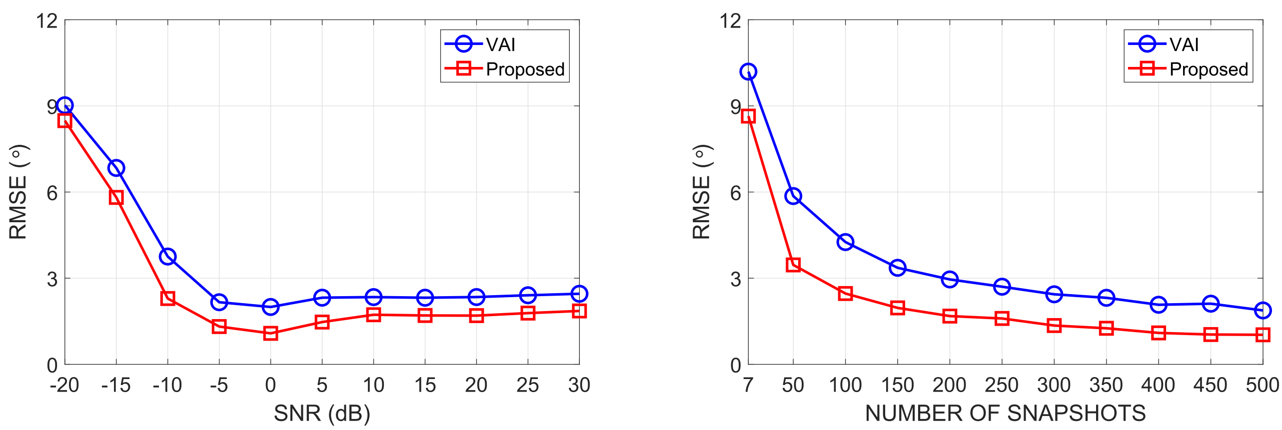

(a) (b)

Fig. 9. DOA estimation accuracy comparison in the maximum achievable DOFs case. (a) RMSE versus SNR when the number of snapshots $L = 500$; (b) RMSE versus the number of snapshots when SNR $= 0$ dB.

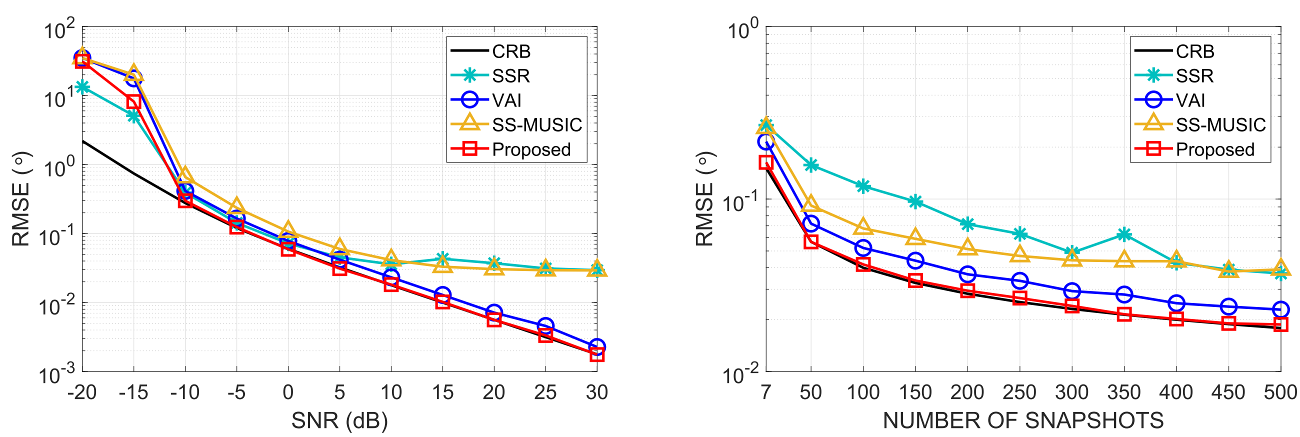

(a) (b)

Fig. 10. DOA estimation accuracy comparison in the overdetermined case with a single random source. (a) RMSE versus SNR when the number of snapshots $L = 500$; (b) RMSE versus the number of snapshots when SNR $= 10$ dB.

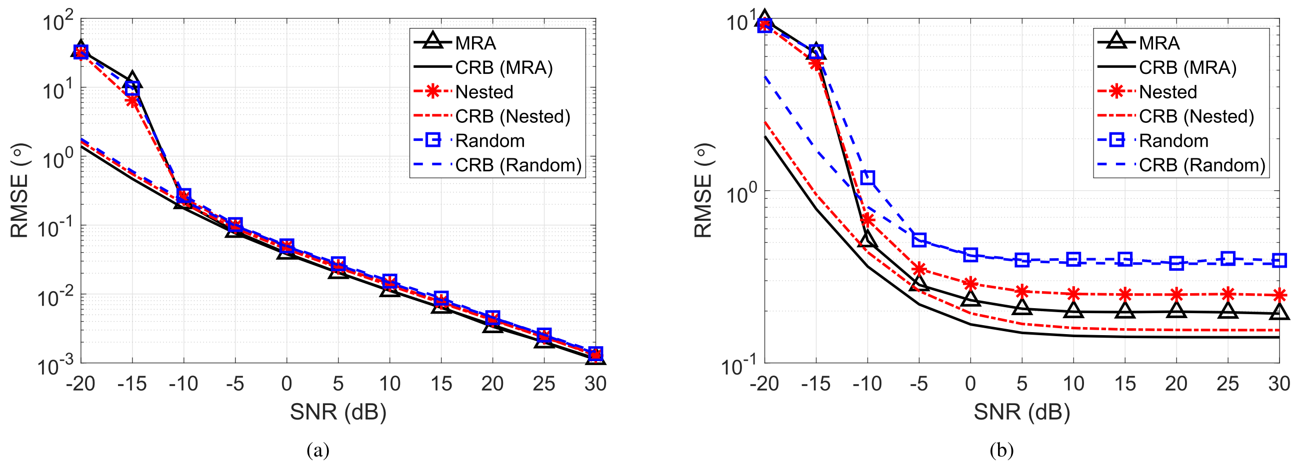

Fig. 11. RMSE versus SNR for the proposed algorithm with different sparse array configurations. (a) Overdetermined case; (b) Underdetermined case.

TABLE II
COMPARISON OF COMPUTATION TIME

Method	SSR	VAI	SS-MUSIC	Proposed
Time (sec)	385.45	300.31	11.81	395.83

$\{0, d, 2d, 3d, 7d, 11d, 15d\}$. For the random sparse array configuration, two sensors are deployed at 0 and $13d$ to maintain a fixed array aperture, while the other five sensors are randomly located at the Nyquist sampling positions between the two end sensors. For the overdetermined case, one single source is assumed to be randomly generated from $\mathcal{N}(0^\circ, 1^\circ)$ trial by trial, whereas for the underdetermined case there are 12 sources uniformly distributed in $[-50^\circ, 50^\circ]$. The parameter setting for the proposed algorithm keeps the same as that in subsection V-C.

It is demonstrated in Fig. 11(a) that the RMSE of the proposed algorithm almost touches the CRB when the SNR is larger than -10 dB in the overdetermined case, regardless of the configuration of the sparse array. In the underdetermined case, when the sparse array configuration varies, the RMSE of the proposed algorithm shown in Fig. 11(b) presents a similar trend as the corresponding CRB. Particularly, for the random sparse array, the RMSE almost overlaps with the CRB when the SNR is larger than -5 dB. Therefore, the proposed Nyquist spatial filling algorithm can be used for effective DOA estimation in conjunction with different sparse array configurations. The CRB difference in Fig. 11 is due to the different array aperture corresponding to each sparse array configuration.

E. Computation Time

In the last simulation, we compare the computational complexity of each algorithm where the parameter setting follows the overdetermined case as simulated in Fig. 10, and the computation time for 500 Monte-Carlo trials on an Intel(R) Core(TM) i7-7600U CPU is listed in Table II. While the SS-MUSIC method does not include any complex optimization process to address the discontiguous virtual array, it has the lowest computation time among the compared methods. By contrast, the computation time for the remaining methods is in the same order. Although the proposed algorithm consumes relatively larger computation time, it achieves more available number of DOFs than the SSR algorithm and outperforms the VAI algorithm in terms of resolution and estimation accuracy. The main complexity of the proposed algorithm lies in the retrieval of whole rows and columns of missing elements in $\tilde{\boldsymbol{R}}_{\boldsymbol{yy}}$, and the principle difference as depicted in Fig. 2 also accounts for the reason on this comparison with the VAI algorithm.

VI. CONCLUSION

In this paper, we proposed a structured correlation reconstruction-based DOA estimation algorithm that is suitable for a general class of sparse linear arrays. By implementing Nyquist spatial filling on the physical array, the structural information is incorporated as a priori to retrieve the whole rows and columns of unknown correlations in its resulting augmented covariance matrix. An equivalence relationship of the estimation performance between the proposed Nyquist spatial filling approach and the virtual array interpolation-based approaches is theoretically established, which is further validated by the Cramér-Rao bound tailored for the proposed algorithm. Numerical simulations indicate that the proposed algorithm maintains the advantages of the sparse arrays and presents a superior performance than the existing sparse array DOA estimation algorithms.

REFERENCES

[1] H. L. Van Trees, *Detection, Estimation, and Modulation Theory, Part IV: Optimum Array Processing*. New York, NY, USA: Wiley, 2002.
[2] Y. Gu and N. A. Goodman, "Information-theoretic compressive sensing kernel optimization and Bayesian Cramér-Rao bound for time delay estimation," *IEEE Trans. Signal Process.*, vol. 65, no. 17, pp. 4525–4537, Sep. 2017.
[3] C. Shi, Y. Wang, S. Salous, J. Zhou, and J. Yan, "Joint transmit resource management and waveform selection strategy for target tracking in distributed phased array radar network," *IEEE Trans. Aerosp. Electron. Syst.*, vol. 58, no. 4, pp. 2762–2778, Aug. 2022.
[4] J. Shi, G. Hu, X. Zhang, F. Sun, W. Zheng, and Y. Xiao, "Generalized co-prime MIMO radar for DOA estimation with enhanced degrees of freedom," *IEEE Sensors J.*, vol. 18, no. 3, pp. 1203–1212, Feb. 2018.
[5] X. Du, A. Aubry, A. De Maio, and G. Cui, "Toeplitz structured covariance matrix estimation for radar applications," *IEEE Signal Process. Lett.*, vol. 27, pp. 595–599, 2020.

[6] Y. Gu and A. Leshem, "Robust adaptive beamforming based on interference covariance matrix reconstruction and steering vector estimation," *IEEE Trans. Signal Process.*, vol. 60, no. 7, pp. 3881–3885, Jul. 2012.
[7] C. Zhou, Y. Gu, Z. Shi, and Y. D. Zhang, "Off-grid direction-of-arrival estimation using coprime array interpolation," *IEEE Signal Process. Lett.*, vol. 25, no. 11, pp. 1710–1714, Nov. 2018.
[8] G. Qin, Y. D. Zhang, and M. G. Amin, "DOA estimation exploiting moving dilated nested arrays," *IEEE Signal Process. Lett.*, vol. 26, no. 3, pp. 490–494, Mar. 2019.
[9] Z. Zheng, Y. Huang, W.-Q. Wang, and H. C. So, "Direction-of-arrival estimation of coherent signals via coprime array interpolation," *IEEE Signal Process. Lett.*, vol. 27, pp. 585–589, 2020.
[10] C. I. Kanatsoulis, X. Fu, N. D. Sidiropoulos, and M. Akçakaya, "Tensor completion from regular sub-Nyquist samples," *IEEE Trans. Signal Process.*, vol. 68, pp. 1–16, 2020.
[11] H. Zheng, Z. Shi, C. Zhou, M. Haardt, and J. Chen, "Coupled coarray tensor CPD for DOA estimation with coprime L-shaped array," *IEEE Signal Process. Lett.*, vol. 28, pp. 1545–1549, 2021.
[12] C. Zhou, Y. Gu, S. He, and Z. Shi, "A robust and efficient algorithm for coprime array adaptive beamforming," *IEEE Trans. Veh. Technol.*, vol. 67, no. 2, pp. 1099–1112, Feb. 2018.
[13] P. P. Vaidyanathan and P. Pal, "Sparse sensing with co-prime samplers and arrays," *IEEE Trans. Signal Process.*, vol. 59, no. 2, pp. 573–586, Feb. 2011.
[14] P. Pal and P. P. Vaidyanathan, "Nested arrays: A novel approach to array processing with enhanced degrees of freedom," *IEEE Trans. Signal Process.*, vol. 58, no. 8, pp. 4167–4181, Aug. 2010.
[15] C.-L. Liu and P. P. Vaidyanathan, "Remarks on the spatial smoothing step in coarray MUSIC," *IEEE Signal Process. Lett.*, vol. 22, no. 9, pp. 1438–1442, Sep. 2015.
[16] Z. Shi, C. Zhou, Y. Gu, N. A. Goodman, and F. Qu, "Source estimation using coprime array: A sparse reconstruction perspective," *IEEE Sensors J.*, vol. 17, no. 3, pp. 755–765, Feb. 2017.
[17] D. G. Chachlakis and P. P. Markopoulos, "Structured autocorrelation matrix estimation for coprime arrays," *Signal Process.*, vol. 183, Jun. 2021, Art. no. 107987.
[18] C. Zhou, Y. Gu, Z. Shi, and M. Haardt, "Direction-of-arrival estimation for coprime arrays via coarray correlation reconstruction: A one-bit perspective," in *Proc. IEEE Sensor Array Multichannel Signal Process. Workshop*, Hangzhou, China, 2020, pp. 1–4.
[19] Y. I. Abramovich, D. A. Gray, A. Y. Gorokhov, and N. K. Spencer, "Positive-definite Toeplitz completion in DOA estimation for nonuniform linear antenna arrays—Part I: Fully augmentable arrays," *IEEE Trans. Signal Process.*, vol. 46, no. 9, pp. 2458–2471, Sep. 1998.
[20] Y. I. Abramovich, N. K. Spencer, and A. Y. Gorokhov, "Positive-definite Toeplitz completion in DOA estimation for nonuniform linear antenna arrays—Part II: Partially augmentable arrays," *IEEE Trans. Signal Process.*, vol. 47, no. 6, pp. 1502–1521, Jun. 1999.
[21] P. Pal and P. P. Vaidyanathan, "Coprime sampling and the MUSIC algorithm," in *Proc. IEEE Digit. Signal Process. Signal Process. Educ. Meeting*, Sedona, AZ, 2011, pp. 289–294.
[22] D. G. Chachlakis, T. Zhou, F. Ahmad, and P. P. Markopoulos, "Minimum mean-squared-error autocorrelation processing in coprime arrays," *Digit. Signal Process.*, vol. 114, Jul. 2021, Art. no. 103034.
[23] E. BouDaher, Y. Jia, F. Ahmad, and M. G. Amin, "Multi-frequency co-prime arrays for high-resolution direction-of-arrival estimation," *IEEE Trans. Signal Process.*, vol. 63, no. 14, pp. 3797–3808, Jul. 2015.
[24] C.-L. Liu, P. P. Vaidyanathan, and P. Pal, "Coprime coarray interpolation for DOA estimation via nuclear norm minimization," in *Proc. IEEE Int. Symp. Circuits Syst.*, Montréal, Canada, 2016, pp. 2639–2642.
[25] S. M. Hosseini and M. A. Sebt, "Array interpolation using covariance matrix completion of minimum-size virtual array," *IEEE Signal Process. Lett.*, vol. 24, no. 7, pp. 1063–1067, Jul. 2017.
[26] C. Zhou, Y. Gu, X. Fan, Z. Shi, G. Mao, and Y. D. Zhang, "Direction-of-arrival estimation for coprime array via virtual array interpolation," *IEEE Trans. Signal Process.*, vol. 66, no. 22, pp. 5956–5971, Nov. 2018.
[27] C. Zhou, Y. Gu, Y. D. Zhang, and Z. Shi, "Coarray interpolation-based coprime array DOA estimation via covariance matrix reconstruction," in *Proc. IEEE Int. Conf. Acoust. Speech, Signal Process*, Calgary, Canada, 2018, pp. 3479–3483.
[28] S. Liu, Z. Mao, Y. D. Zhang, and Y. Huang, "Rank minimization-based Toeplitz reconstruction for DoA estimation using coprime array," *IEEE Commun. Lett.*, vol. 25, no. 7, pp. 2265–2269, Jul. 2021.
[29] S. Qin, Y. D. Zhang, and M. G. Amin, "Generalized coprime array configurations for direction-of-arrival estimation," *IEEE Trans. Signal Process.*, vol. 63, no. 6, pp. 1377–1390, Mar. 2015.
[30] Q. Shen, W. Liu, W. Cui, S. Wu, and P. Pal, "Simplified and enhanced multiple level nested arrays exploiting high-order difference co-arrays," *IEEE Trans. Signal Process.*, vol. 67, no. 13, pp. 3502–3515, Jul. 2019.
[31] R. Rajamaki and V. Koivunen, "Sparse symmetric linear arrays with low redundancy and a contiguous sum co-array," *IEEE Trans. Signal Process.*, vol. 69, pp. 1697–1712, Feb. 2021.
[32] G. Qin, M. G. Amin, and Y. D. Zhang, "DOA estimation exploiting sparse array motions," *IEEE Trans. Signal Process.*, vol. 67, no. 11, pp. 3013–3027, Jun. 2019.
[33] X. Wang, A. Hassanien, and M. G. Amin, "Dual-function MIMO radar communications system design via sparse array optimization," *IEEE Trans. Aerosp. Electron. Syst.*, vol. 55, no. 3, pp. 1213–1226, Jun. 2019.
[34] Z. Mao, S. Liu, Y. D. Zhang, L. Han, and Y. Huang, "Joint DoA-range estimation using space-frequency virtual difference coarray," *IEEE Trans. Signal Process.*, vol. 70, pp. 2576–2592, 2022.
[35] E. J. Candès and Y. Plan, "Matrix completion with noise," *Proc. IEEE*, vol. 98, no. 6, pp. 925–936, Jun. 2010.
[36] D. Malioutov, M. Çetin, and A. S. Willsky, "A sparse signal reconstruction perspective for source localization with sensor arrays," *IEEE Trans. Signal Process.*, vol. 53, no. 8, pp. 3010–3022, Aug. 2005.
[37] Y. D. Zhang, M. G. Amin, and B. Himed, "Sparsity-based DOA estimation using co-prime arrays," in *Proc. IEEE Int. Conf. Acoust., Speech, Signal Process.*, Vancouver, Canada, 2013, pp. 3967–3971.
[38] C. Zhou, Y. Gu, Y. D. Zhang, Z. Shi, T. Jin, and X. Wu, "Compressive sensing-based coprime array direction-of-arrival estimation," *IET Commun.*, vol. 11, no. 11, pp. 1719–1724, Aug. 2017.
[39] H. Zheng, C. Zhou, Z. Shi, and Y. Gu, "Structured tensor reconstruction for coherent DOA estimation," *IEEE Signal Process. Lett.*, vol. 29, pp. 1634–1638, 2022.
[40] X. Wu and W.-P. Zhu, "On efficient gridless methods for 2-D DOA estimation with uniform and sparse L-shaped arrays," *Signal Process.*, vol. 191, Feb. 2022, Art. no. 108351.
[41] Z. Yang, J. Li, P. Stoica, and L. Xie, "Sparse methods for direction-of-arrival estimation," in *Academic Press Library in Signal Processing*, Cambridge, MA, USA: Academic Press, 2018, pp. 509–581.
[42] X. Wu, W.-P. Zhu, and J. Yan, "A high-resolution DOA estimation method with a family of nonconvex penalties," *IEEE Trans. Veh. Technol.*, vol. 67, no. 6, pp. 4925–4938, Jun. 2018.
[43] A. J. Weiss and B. Friedlander, "Performance analysis of spatial smoothing with interpolated arrays," *IEEE Trans. Signal Process.*, vol. 41, no. 5, pp. 1881–1892, May 1993.
[44] P. Stoica and A. Nehorai, "MUSIC, maximum likelihood, and Cramér-Rao bound: Further results and comparisons," *IEEE Trans. Acoust., Speech, Signal Process.*, vol. 38, no. 12, pp. 2140–2150, Dec. 1990.
[45] C.-L. Liu and P. P. Vaidyanathan, "Cramér-Rao bounds for coprime and other sparse arrays, which find more sources than sensors," *Digit. Signal Process.*, vol. 61, pp. 43–61, Feb. 2017.
[46] M. Wang and A. Nehorai, "Coarrays, MUSIC, and the Cramér-Rao bound," *IEEE Trans. Signal Process.*, vol. 65, no. 4, pp. 933–946, Feb. 2017.
[47] Z. Zhang, Z. Shi, and Y. Gu, "Ziv-Zakai bound for DOAs estimation," *IEEE Trans. Signal Process.*, vol. 71, pp. 136–149, 2023.
[48] B. D. Rao and K. V. S. Hari, "Performance analysis of root-MUSIC," *IEEE Trans. Acoust., Speech, Signal Process.*, vol. 37, no. 12, pp. 1939–1949, Dec. 1989.

Chengwei Zhou (Member, IEEE) received the Ph.D. degree in electronic science and technology from Zhejiang University, Hangzhou, China, in 2018. He was a Visiting Researcher with the University of Technology Sydney, Sydney, NSW, Australia, from April 2017 to October 2017. He was a Postdoctoral Research Fellow with the State Key Laboratory of Industrial Control Technology, the College of Control Science and Engineering, Zhejiang University, from 2018 to 2020. Since June 2020, he has been a Research Associate Professor with the College of Information Science and Electronic Engineering, Zhejiang University. His research interests include array signal processing, direction-of-arrival estimation, and adaptive beamforming.

Dr. Zhou serves as an Associate Editor for *International Journal of Communication System*s, and the Editorial Board Member of *Journal of Signal Processing* (in Chinese). He was the recipient of the 2021 IEEE Signal Processing Society Young Author Best Paper Award, ISAP 2020 Best Paper Award, and 2019 IET Communications Premium Award.

Yujie Gu (Senior Member, IEEE) received the Ph.D. degree in electronic engineering from Zhejiang University, Hangzhou, China, in 2008. After graduation, he held multiple research positions in China, Canada, Israel, and the USA. He is currently a Senior Radar Scientist with Aptiv, Agoura Hills, CA, USA. His research interests include statistical and array signal processing.

Currently, he is the Subject Editor-in-Chief for *Electronics Letters* and an Associate Editor for *Signal Processing*. He was the Lead Guest Editor of the Special Issue on "Source Localization in Massive MIMO" for *Digital Signal Processing*. He is an Elected Member of the Sensor Array and Multichannel (SAM) Technical Committee and the Signal Processing Theory and Methods (SPTM) Technical Committee of the IEEE Signal Processing Society. He was the Special Sessions Co-Chair of the 2020 IEEE Sensor Array and Multichannel Signal Processing Workshop. Dr. Gu was the recipient of the 2019 IET Communications Premium Award, and coauthored a paper that was the recipient of the 2021 IEEE Signal Processing Society Young Author Best Paper Award.

Zhiguo Shi (Senior Member, IEEE) received the B.S. and Ph.D. degrees in electronic engineering from Zhejiang University, Hangzhou, China, in 2001 and 2006, respectively. Since 2006, he has been a Faculty Member with the College of Information Science and Electronic Engineering, Zhejiang University, where he is currently a Full Professor. From 2011 to 2013, he visited the Broadband Communications Research Group, University of Waterloo, Waterloo, ON, Canada. His research interests include array signal processing, localization, and internet-of-things.

He was the recipient of the 2019 IET Communications Premium Award, and coauthored a paper that was the recipient of the 2021 IEEE Signal Processing Society Young Author Best Paper Award. He was also the recipient of the Best Paper Award from ISAP 2020, IEEE GLOBECOM 2019, IEEE WCNC 2017, IEEE/CIC ICCC 2013, and IEEE WCNC 2013. He was the General Co-Chair of IEEE SAM 2020 and was the Editor of the IEEE NETWORK and *IET Communications*. Dr. Shi is currently an Associate Editor for the IEEE SIGNAL PROCESSING LETTERS, IEEE TRANSACTIONS ON VEHICULAR TECHNOLOGY, and *Journal of the Franklin Institute*. He is an Elected Member of the Sensor Array and Multichannel (SAM) Technical Committee of the IEEE Signal Processing Society.

Martin Haardt (Fellow, IEEE) received the Diplom-Ingenieur (M.S.) degree from the Ruhr-University Bochum, Bochum, Germany, in 1991, and the Doktor-Ingenieur (Ph.D.) degree from the Munich University of Technology, Munich, Germany, in 1996. He has been a Full Professor with the Department of Electrical Engineering and Information Technology and the Head of the Communications Research Laboratory, Ilmenau University of Technology, Germany, since 2001. After studying electrical engineering with Ruhr-University Bochum, and with Purdue University, West Lafayette, IN, USA, In 1997, he joint Siemens Mobile Networks in Munich, where he was responsible for strategic research for third generation mobile radio systems. From 1998 to 2001, he was the Director for International Projects and University Cooperations in the mobile infrastructure business of Siemens in Munich, where his work focused on mobile communications beyond the third generation. His research interests include wireless communications, array signal processing, high-resolution parameter estimation, as well as tensor-based signal processing. Martin Haardt was the recipient of the 2009 Best Paper Award from the IEEE Signal Processing Society, the Vodafone Innovations Award for outstanding research in mobile communications, the ITG Best Paper Award from the Association of Electrical Engineering, Electronics, and Information Technology (VDE), and the Rohde & Schwarz Outstanding Dissertation Award.

Dr. Haardt has served as a Senior Editor for IEEE JOURNAL OF SELECTED TOPICS IN SIGNAL PROCESSING (since 2019), an Associate Editor for the IEEE TRANSACTIONS ON SIGNAL PROCESSING (2002–2006 and 2011–2015), the IEEE SIGNAL PROCESSING LETTERS (2006–2010), the *Research Letters in Signal Processing* (2007–2009), *Hindawi Journal of Electrical and Computer Engineering* (since 2009), *EURASIP Signal Processing Journal* (2011–2014), and a Guest Editor for the *EURASIP Journal on Wireless Communications and Networking*. From 2011 to 2019, he was an Elected Member of the Sensor Array and Multichannel (SAM) Technical Committee of the IEEE Signal Processing Society, where he was the Vice Chair (2015–2016), Chair (2017–2018), and Past Chair (2019). Since 2020, he has been an Elected Member of the Signal Processing Theory and Methods (SPTM) Technical Committee of the IEEE Signal Processing Society. He was the Technical Co-Chair of PIMRC 2005 in Berlin, Germany, ISWCS 2010 in York, UK, the European Wireless 2014 in Barcelona, Spain, and the Asilomar Conference on Signals, Systems, and Computers 2018, USA, and the General Co-Chair of WSA 2013 in Stuttgart, Germany, ISWCS 2013 in Ilmenau, Germany, CAMSAP 2013 in Saint Martin, French Antilles, WSA 2015 in Ilmenau, Germany, SAM 2016 in Rio de Janeiro, Brazil, CAMSAP 2017 in Curaçao, Dutch Antilles, SAM 2020 in Hangzhou, China, and the Asilomar Conference on Signals, Systems, and Computers 2021, USA.